AUTONOMIC THERMAL SWITCH BASED ON PHASE TRANSITION ALLOYS

BY

XUEJIAO LI

THESIS

Submitted in partial fulfillment of the requirements
for the degree of Master of Science in Materials Science and Engineering
in the Graduate College of the
University of Illinois at Urbana-Champaign, 2017

Urbana, Illinois

Adviser:

Professor Paul Braun

ABSTRACT

Thermal management opens the new era of next generation electronic and thermal devices. Research on nano-scaled autonomic thermal switching is lacking because the suitable material is hard to synthesis. Our approach is utilizing the phase change property of eutectic/eutectoid materials. Triggered by heat, this type of material is possible to be directionally solidified into anisotropic structure, such as ordered lamellae and rods. We have surveyed the whole family of binary eutectic and eutectoid alloys and come up with a few good candidates for thermal switching applications. Two of the materials we studied in this thesis are Cu-P-Ag alloy and Cu-P eutectic alloy. The experimental methods we use are directional solidification and Time-domain Thermo-reflectance (TDTR) measurement. We have achieved large area of ordered lamellar structure up to hundreds of micron meters using Cu-P eutectic alloy. We include a few modern techniques to study the composition of both materials, which could be applied to other candidates for this type of application. The thermal conductivities of both materials are measured using TDTR. The Cu-P-Ag alloy and Cu-P eutectic alloy have thermal conductivity of 13.34 W/mK and 8.23 W/mK respectively. The theoretical estimation of thermal conductivity of Cu-P-Ag is around 40 W/mK, and the theoretical estimation for Cu-P eutectic alloy is around 200 W/mK. Both of our measured values are a little off from our estimated thermal conductivity of composite alloys, but the directional solidified alloys of these typies were not measured before. It may due to the fact of surface reaction of our alloys with the environment and caused oxidation and contamination, and TDTR is a surface sensitive technique for thermal conductivity measurment. Other possible thermal measurements like Scanning Thermal Microscopy (SThM) and 3-omega thermal measurement should be included as a comparison in future.

ACKNOWLEDGMENTS

I am truly thankful to have Prof. Paul Braun as my academic advisor through all the years I am a student at University of Illinois at Urbana-Champaign. He is an amazing scientist with vast interdisciplinary knowledge. He is always kind, supportive, and inspiring, and cares a lot about the progress of my work. My co-advisor Prof. David Cahill, a well-known expert in the thermal area, gives me lots of useful guide on how to solve difficulties when I am stuck with my research. He has always been easy to reach out and gave me suggestions beyond the thermal area, which I appreciate a lot.

I would also like to thank my colleagues Ashish Kulkarni, who is an expert in the area of directional solidification. He trained me on a lot of the equipment in our lab, and our discussions about the methodologies and plans of my project are very helpful. Julia Kohanek and Kaitlin Tyler also did a lot of meetings with me to discuss the approaches and directions of my research that helped me started in an area I never knew before. Many thanks to Jin Gu Kang, who is a great friend and collaborator in several of my projects. He leads me into critical thinking about scientific studies. I appreciate Jungwoo Shin's help and references when we did the POETS annual projects together. Dr. Pengcheng Sun, who will keep my project going in future, gives me useful information based on his rich experience in thermal switching area. I was also very fortunate to work with Qiye Zheng during my study at University of Illinois. He not only trained me on how to use TDTR, but also pointed out the odds and errors happened with my experiment when I am with sets of data or apparatus arrangements.

Acknowledgement also goes to the stuff members at MRL with responsible training, and for maintaining a pleasant working environment. Special thanks to Dr.

Honghui Zhou, Dr. Mauro Sardela, Dr. Julio Soares, and Dr. Changqiang Chen. They all trained me on some of the equipment at MRL with great patience and effort. Also, thanks to my funding from POETS grand.

I can never finish my study with my family. My parents are supportive about my study in the US and helped me take care of my daughter while I just started grad school. I would not have the energy to keep up with everything without their help. Thanks to Alyssa, who is the sweetest daughter I could ever have, for all the joy she brings to our family. Last but not least, I must thank my dear husband. His encouragement keeps moving forward through the difficult times in life, and thanks to his continued and unfailing love to make this thesis possible.

TABLE OF CONTENTS

CHAPTER 1

INTRODUCTION

1.1 Eutectic/Eutectoid Materials and Directional Solidification

A thermal switch controls the heat transport in a device, and it turns on/off the thermal or electrical circulation when a trigger is given. The types of trigger can be heat, voltage, chemical reaction, and so on depending on different applications. As a safety feature of the entire device, thermal switch plays a crucial role. The fast development of the electro-thermal devices puts an urge for seeking the next generation's micro/nano-scaled thermal switches. The main focus of current research is on more renovation materials and based on more reliable and simple mechanisms. Our design of high thermal conductivities switching is based on directional solidified eutectic/eutectoid materials, which provide the device with phase change and anisotropic structure.

Eutectic/Eutectoid materials are mixtures of two or more components in such portions that the melting temperatures of the eutectic/eutectoid materials are lower than the mixing components themselves [1]. Many eutectic alloys are traditionally used for soldering due to the low melting temperatures, such as Tin-Silver-Copper (TSC), Copper-Zinc (Cu-Zn), and Tin-Lead-Silver (Sn-Pb-Ag) [2]. A typical phase diagram of eutectic material is shown in Figure 1. The eutectic melting temperature of the alloy is defined as T_E. Above the eutectic melting temperature, the phases are separated by two liquidus lines, which include a completely liquid phase straight above the eutectic composition point E. Below the eutectic composition, two solid phases of A and B are coexisted [3]. The phase diagram of a eutectoid material is similar to a eutectic phase diagram except that in the liquidus phase is replaced by another solidus phase.

To illustrate the characteristics of eutectic and eutectoid phase diagrams, we can use the steel part of the phase diagram of Iron-Carbon (Fe-C) shown in Figure 2 [4]. At the eutectoid temperature 727 ^{o}C with 0.76 wt% Carbon, the two solid phases below the eutectoid temperature is α-ferrite and iron carbide (Fe_3C), and the single solid phase above the eutectoid temperature is γ-austenite. At the eutectic temperature of 1147 ^{o}C and with 4.3 wt% of carbon, two solid phases of γ-Fe and Fe_3C form into a liquid phase above the eutectic temperature. The microstructures of Fe-C alloy are one of the most widely studied in the world, and the applications go far beyond the industrial field.

Recent years, lots of research projects are focused on toning the structure of eutectic alloys systematically and finding innovative applications to substitute traditional materials. For example, LiF-$LiYF_4$ is directional solidified in 2013 and shows very good optical property [21]. Al-Zn-Cu, another traditional eutectic alloy, is directionally solidified into ordered lamellae and shows some good mechanical properties in 2015 [5]. The artificial fabricated optical material, terbium-scandium-aluminum and terbium-scandium eutectic alloys show strong Faraday effect [6]. Although there are lots of open questions about eutectic materials, the potential of these types of eutectic structures are unlimited and worth researching.

Two-phase eutectic/eutectoid materials can form different structures based on composition and solidification thermal gradient (pulling speed). Types of structures are lamellar, rod-like, globular, and acicular as shown in Figure 3 [7]. The lamellar and rod-like structures are suitable for the application of thermal switch because of the directionality of the phases, which is unlike the globular and acicular structures that are isotropic in all directions. To find materials having such property, we use an experimental technique called directional solidification. When eutectic material is solidified under certain thermal gradient, we can have control about the

resulting structures. For example, the lamellar structure spacing and the continuity of the lamellar structure, and resulting in anisotropic thermal conductivity [8,9].

1.2 Autonomic Thermal Switch Based on Anisotropic Material

The traditional thermal switches are usually designed for one-time use, and are for large machines and devices [10]. For example, the fire sprinkler is one kind of thermal switches triggered by temperature. When the surroundings have a temperature higher than the melting point of the thermal switch material, water can be turned on [11]. However, as electronic devices getting smaller and smaller, the nano-scaled thermal switches become an urge to the whole technology field for guarantee the safety of the entire device. The next generation's thermal switch should fit into a nano-sized device, and have the property of repeatable usage due to the fact that replacing a small fixture in a high-tech device is challenging. Therefore, eutectic/eutectoid materials would be good candidates for this kind of applications.

For the purpose of finding thermal switching material, we surveyed all the binary eutectic materials with high contrast of thermal conductivities. The phases of material consisted by metal-nonmetal and metal-semiconductors phases would naturally give the anisotropic thermal conducting properties in different directions if a self-assembled ordered structure of the phases can be realized, eg. high thermal conductivity along the growth direction of the phases and low thermal conductivity perpendicular to the growth direction of the phases. In addition, the thermal conductivity can also be changed dramatically triggered by temperature due to phase change, eg. low thermal conductivity in the solid phase and high thermal conductivity in the liquid phase, or vise versa.

Previously, a few nano scaled thermal switches published shows reasonable switching ratio, however, the repeatability of many thermal switches are based on mechanically moving the material through changing contact. For example, a vapor-liquid phase change thermal switch has a switching ratio of one order of magnitude has developed by Ng et al in 2016 [12]. In this work, we focus on the anisotropic thermal conductivity of eutectic materials, and the directional solidification process of our material, in order to study eutectic/eutectoid materials' potential as thermal switches.

1.3 Time-domain Thermoreflectance

Time-domain Thermoreflectance (TDTR) is a popular and advanced technique that uses laser to measure the thermal conductivity of thin film, bulk, super-lattice and wire. It is a pump-probe technique that one beam of laser is served as a pump beam to heat up the material, and the other beam of laser is served as a probe beam to measure the change of thermal reflectivity of the sample [13]. The surface of the sample itself has to be polished smoothly to optical degree, and a metal transducer (usually aluminum) needs to be deposited on top of the polished surface. Since the thermal reflectivity on the surface is correlated with the thermal conductivity, the output signal generated by the rf lock-in amplifier has a in phase component V_{in} and a out of phase component V_{out}. We can do a series of calculation based on the thermal diffusion equation using known values of film thickness and heat capacity to get the thermal conductivity with high accuracy in this way.

The schematic setup of our TDTR equipment is shown in Fig. 2 [14]. A Tsunami Ti:Sapphire laser with a tuning range of 720-850 nm was used to produce pulses (<400 ps) for the pump and probe. A polarized beam splitter (PBS) is used to orthogonally split the beam into

the pump beam and a probe beam. A spectrum analyzer is used to modulate the wavelength of the beam to be at 783 nm and the full width at half maximum (FWHM) at 10 nm. The power ratio between the pump and the probe beam is typically controlled to be 2 to 1 using the PBS and a half wave plate. An electro-optical modulator is used to control the intensity of the pump beam with frequency of 10.1 MHz [15]. For our experiment, the pump and probe beams are tuned to be 10 mV and 5 mV respectively. A double modulation technique of combining a lock-in amplifier and a mechanical chopper is used to increase the accuracy of our TDTR setup.

An alternative method for TDTR is 3ω thermal conductivity measurement. It suits measurement for bulk and thin film materials. A schematic diagram of the 3ω method is shown in Figure 5 [16]. A thin metallic wire shown in yellow color is deposited on top of the sample, and is used as an electrical heater and a temperature sensor. An alternative current (AC) is running through the wire from two long ends at frequency of ω, and it causes a heating at 2ω frequency. Coupled with the electrical resistance of the wire, a voltage changes at 3ω can be measured at the two short ends of the wire [17]. The length L shown in Fig. 5.a) is usually between 1000 and 10000 μm, and the half width length a shown in Fig. 5.b) is usually between 10 and 50 μm [18]. One of the significant advantages of the 3ω thermal conductivity measurement is that we can control the penetration depth by changing the frequency ω, which usually works better for thick samples than TDTR [19].

1.4 Figures

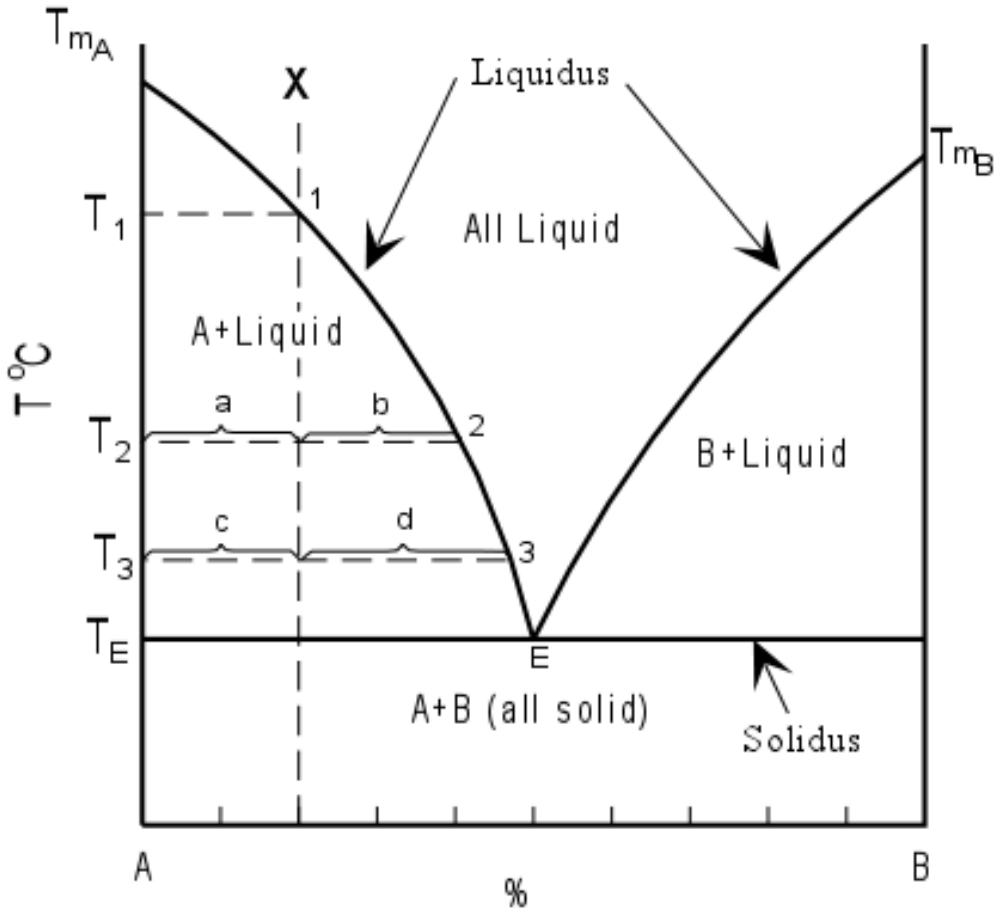

Figure 1: Phase diagram of a typical eutectic material composited by element A and element B.

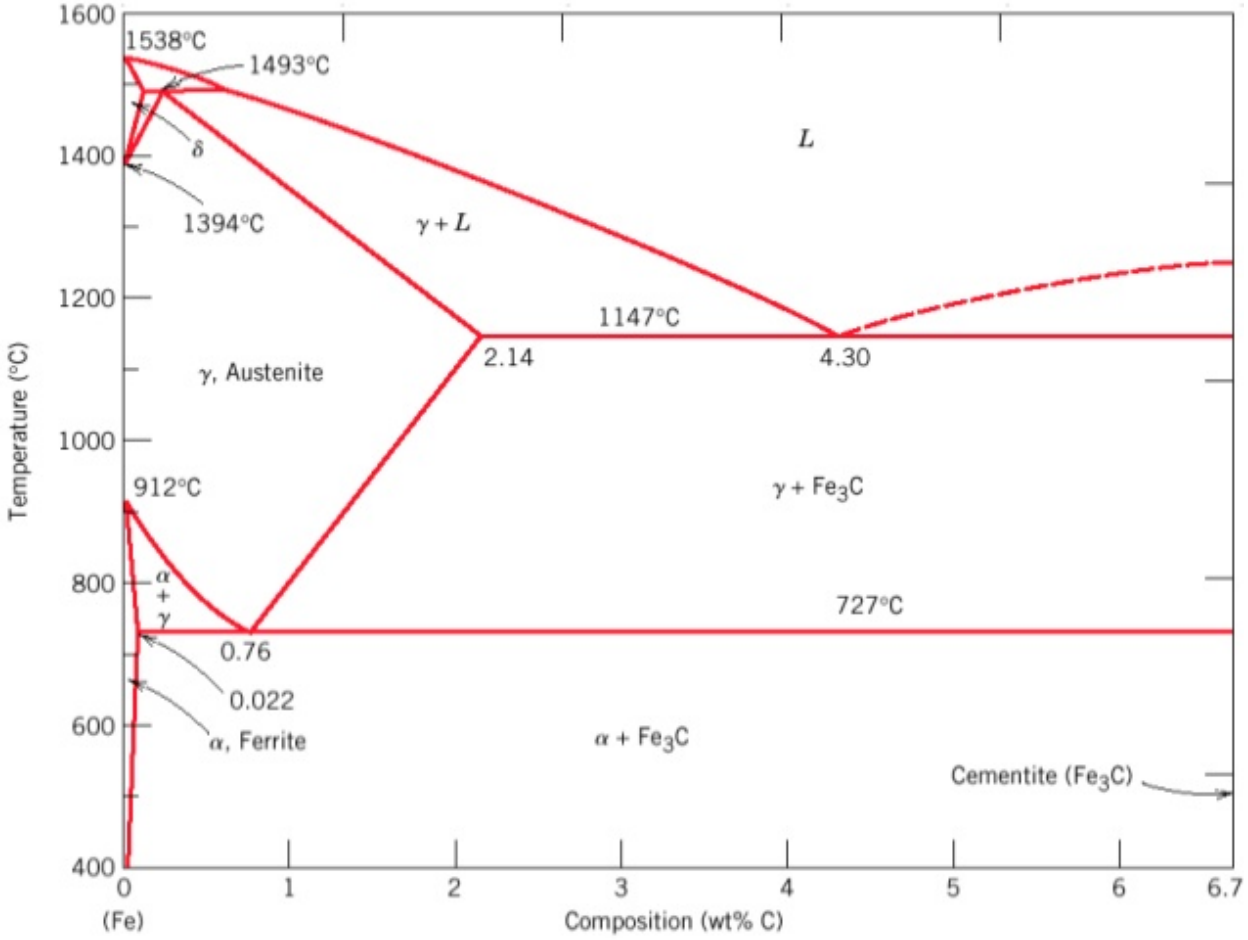

Figure 2: The phase diagram of Fe-C with carbon concentration up to 6.7 wt%.

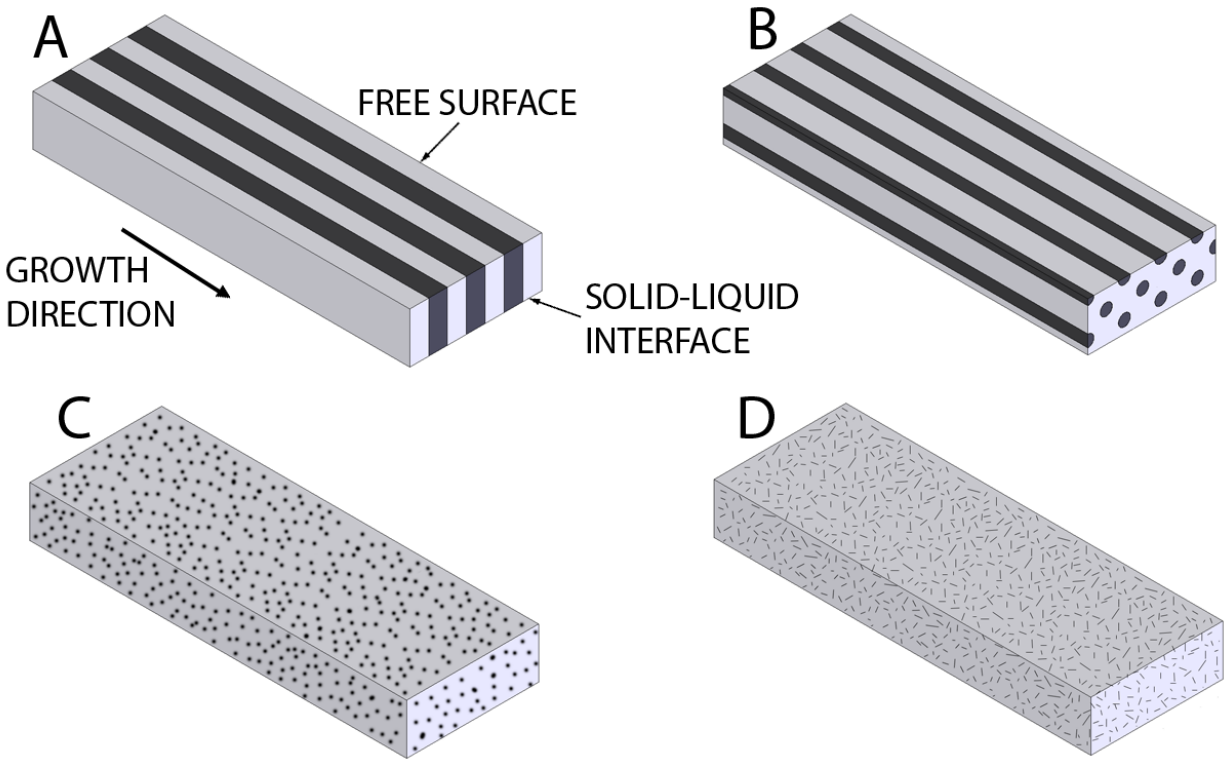

Figure 3: Different kinds of eutectic structure (A) Lamellar (B) Rod-like (C) Globular (D) Random

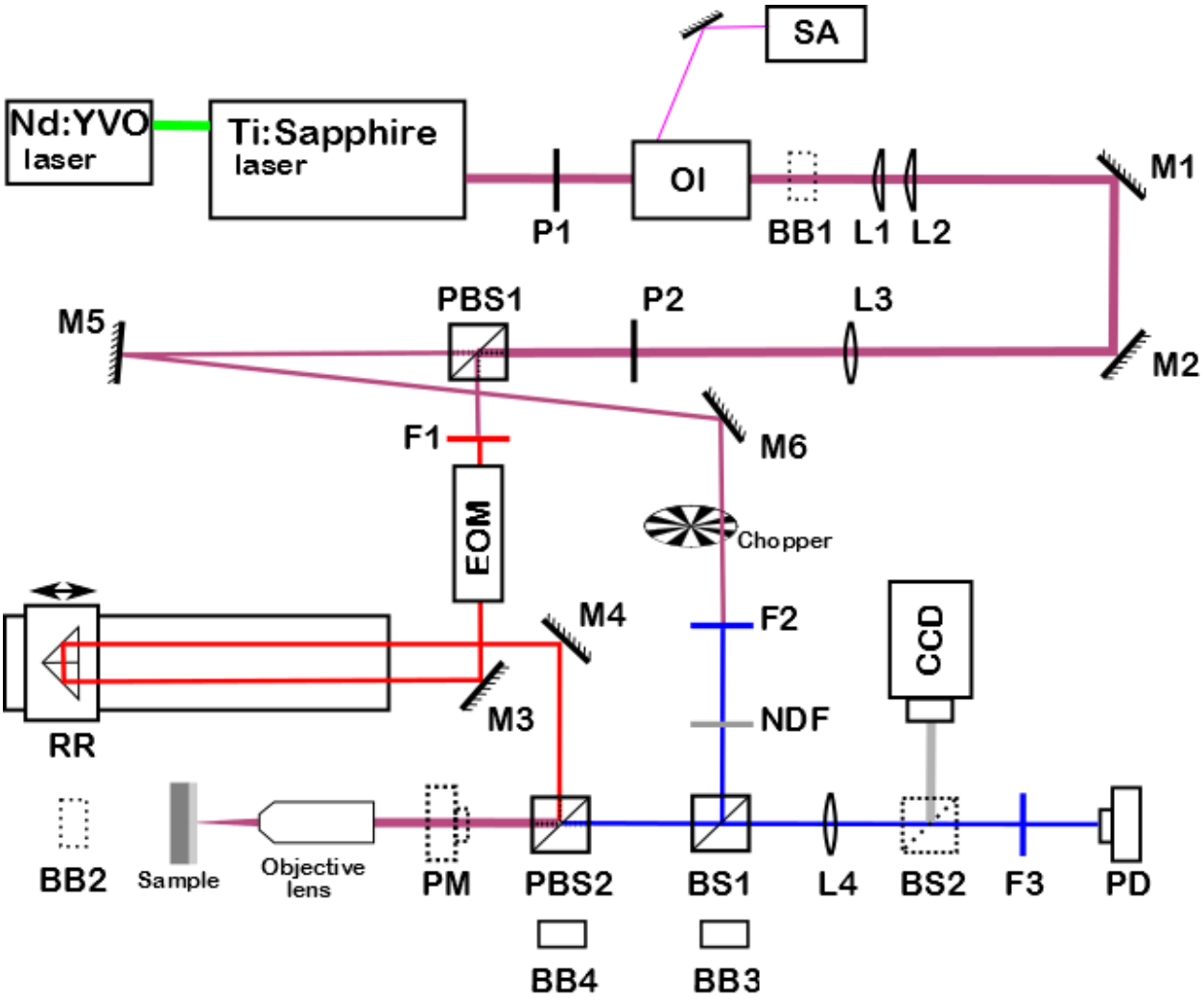

Figure 4: The schematic diagram of a TDTR setup.

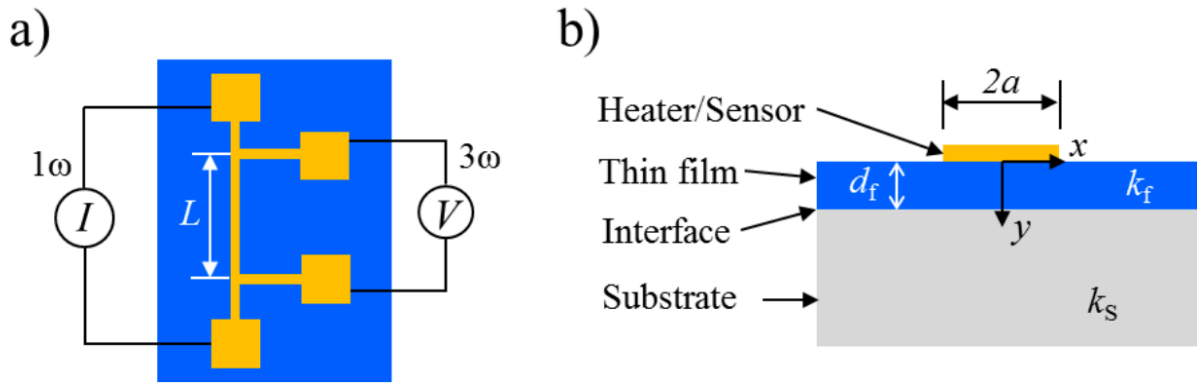

Figure 5: The schematic diagram of 3ω method a) top view, b) cross-section of the metal wire deposited on thin film.

CHAPTER 2

BINARY EUTECTIC AND EUTECTOID CANDIDATES SELECTION

2.1 Background

The traditional thermal switch relies a lot on mechanical type of trigger to disconnect the thermal pathway, and not much on designs of autonomic switching materials [20]. These types of switches have limited application because they need to be reset or changed after using it once. In addition, in a highly integrated device, the whole unit has to be replaced once the thermal switch is used, which is not economical and time efficient. One example of traditional thermal switch is made via bimetallic strip materials [21]. The bimetallic materials have two layers of different metals, of which have very different amount of thermal expansions upon heating or cooling, therefore, the thermal switching device mechanically snaps at certain temperature to cut off or connect the thermal circuit.

For the next generation's thermal switch, people focused on a lot about phase changing materials, which have merits like, size tunable to nano-scale, reusability, cost efficient, and different switching temperature windows since the year 2010 [22]. A group of researchers at Aarhus University have found the thermal conductivity switching property of one single string of DNA at 70 ^{o}C [23]. However, the practical application of biomaterial like DNA is difficult to integrate into an actual device, and the cyclability of DNA is questionable in high technological electronics. More recently, a phase change thermal switch is innovated by graphene coating published in 2016, but the actual device is no difference than the traditional mechanical thermal switches relied on different thermal expansion rates [12]. Hence, developing a new type of

thermal switch based on phase changing, and having an intrinsic anisotropic thermal conductivity is much more practical than the current developed nano-thermal switching systems.

2.2 The Structural and Thermal Properties of Eutectic Candidates

While most current research focuses on the phase transition between solid, liquid, and gas phases to increase the thermal conductivity contrast, our goal is to increase the thermal conductivity contrast of ordered eutectic structures in the solid phase. For example, the lamellar structure of a directional solidified bulk material shows high thermal conductivity along the direction of the lamellar structure, but low thermal conductivity in the cross plane of the lamellar structure. The reason is duo to different thermal conductivities of the two phases consisting the lamellar structures, and also the boundary thermal conductivity.

Considering the eutectic temperature, the lamellar structure, and the thermal conductivities of the phases, we have surveyed all the possible binary alloys [24,25]. We choose a few candidates for eutectic alloys that form liquid phase above the eutectic temperatures, and form solid phases below the eutectic temperature.

Copper Phosphorous (Cu-P) eutectic alloy with 8.38% phosphor concentration is one of our best candidates so far. Its eutectic temperature is 714 ^{o}C. The phase diagram is shown in Figure 6, from which we can see that the solid phase is consisted by a copper rich α phase and a Cu_3P phase [26]. The thermal conductivity of copper is relatively high in the periodic table at 386 W/mK at room temperature [27]. The thermal conductivity of Cu_3P is unknown, but we found that it is a semi-conducting metal, which means its thermal conductivity should be a lot lower than copper [28]. Moreover, Cu-P eutectic alloy is one of the few eutectic systems that does not grow dendrites easily, which gives us more freedom on the directional solidification

experiment. It is also not expensive and earth abounded. Therefore, we started our investigation from this alloy even though its eutectic temperature is higher than what we actually expected for our current lab set-up, and the transition temperature is very high served as a thermal switch.

Another interesting candidate is eutectic alloy Barium Copper (Ba-Cu) shown in Figure 7. Barium (Ba) has a relatively low thermal conductivity of 18.6 W/mK among metals and a body centered cubic (BCC) structure, while copper's thermal conductivity is twenty times higher than Ba [29]. Among the system's eutectic temperatures, we find that the one at 458 ^{o}C is useful with the concentration of Ba at 79.4%. The two phases are BaCu with a hexagonal structure, and a Ba rich phase [30]. The limitation of this alloy is that it is very reactive in air, so the safety of our thermal device and the experimental difficulty have to be considered if we use this material.

Other favorable materials in this category include Phosphor Tin, Phosphor Platinum, and Bismuth Patassium eutectic alloys. They all form two phases of one metal rich phase and the other semi-conducting phase at the eutectic composition. Theoretically, these candidates can all form high contrast in thermal conductivities of different phases. However, the thermal properties and eutectic structures are rarely studied experimentally before. Therefore, researching on these candidates for thermal switching applications are necessary in future.

2.3 The Structural and Thermal Properties of Eutectoid Candidates

Besides eutectic material, another even better choice of materials that are easy to be integrated into devices are eutectoid materials. The reason is that the eutectoid transition is happened so that two or more solid phases become a single solid phase upon the eutectoid temperature, which would be easier and safer to integrate into a thermal circuit than eutectic materials. After searching all the binary metal alloys, we find that unlike eutectic materials, some

of which have quite low eutectic temperatures (like solder alloys), eutectoid transitions usually happen at very high temperatures [24,25]. Some of the good examples could be used for thermal switches are Titanium-Aluminum (Ti-Al), Manganese-Molybdenum (Mn-Mo), Manganese-Titanium (Mn-Ti), Manganese-Zinc (Mn-Zn), and Titannium-Tungsten (Ti-W).

Ti-Al has a small window of eutectoid at 1125 ^{o}C with 40.4 at% Al content, which is hard to achieve experimentally, but we find an interesting phase transition with slightly more Al content than the eutectoid composition with lamellar structures shown in Figure 8 as the horizontal line crossing temperature at 1125 ^{o}C. In this window, Below 1125 ^{o}C, two of the phases consisting the lamellar structures are γ and Ti_3Al, and above this eutectoid temperature, the lamellae becomes α and γ phases [31]. Since α is rich in Ti, which has a very low thermal conductivity of 20 W/mK, and Ti_3Al with a higher concentration of Aluminum (thermal conductivity of 237 W/mK), we would expect the difference in thermal conductivity facilitates thermal switching properties [32].

Mn-Mo's eutectoid temperature is at 1383 ^{o}C, and the composition of Mo is at 35.7% with a small stoichiometry range shown in Figure 9. The σ phase is studied to have a model of $Mn_{10}Mo_4(Mn,Mo)_{16}$ and in the space group of $P4_2$. The μ phase has a model of $Mn_7Mo_2Mo_4$ and space group of R3m, and cbcc phase has a model of $(Mn,Mo)_1$ with the space group of I43m [33]. Nevertheless, there is no literature about the thermal properties of these phases. It might be interesting to study the thermal properties with mathematic models and predict the behavior of each phase before experimental research. Therefore, it could also be an interesting candidate for thermal switches.

Last but not least, we want to give the most credibility in the eutectoid category to Mn-Zn because it has eutectoid transitions at three different temperatures with different ratios of Mn and

Zn shown in Figure 10. The eutectoid temperatures are at 220, 530, and 620 ^{o}C separately [34]. The elemental Mn has very low thermal conductivity of 7 W/mK, and in contrast, Zn is a very good thermal conducting material with thermal conductivity of 116 W/mK [35]. In addition, there are three single-phase transitions at temperatures of 180, 270, and 530 ^{o}C separately. Hence, if we have the opportunity of synthesizing this material in our lab, trying different combinations of Mn and Zn would give us lots of opportunity and show promising results as well.

To sum up, there are lots of promising candidates for phase change triggered thermal switches, and there must be more choices beyond binary alloys. For future studies, the direction should be researching on this particular area using machine learning on large material science data base.

2.4 Figures

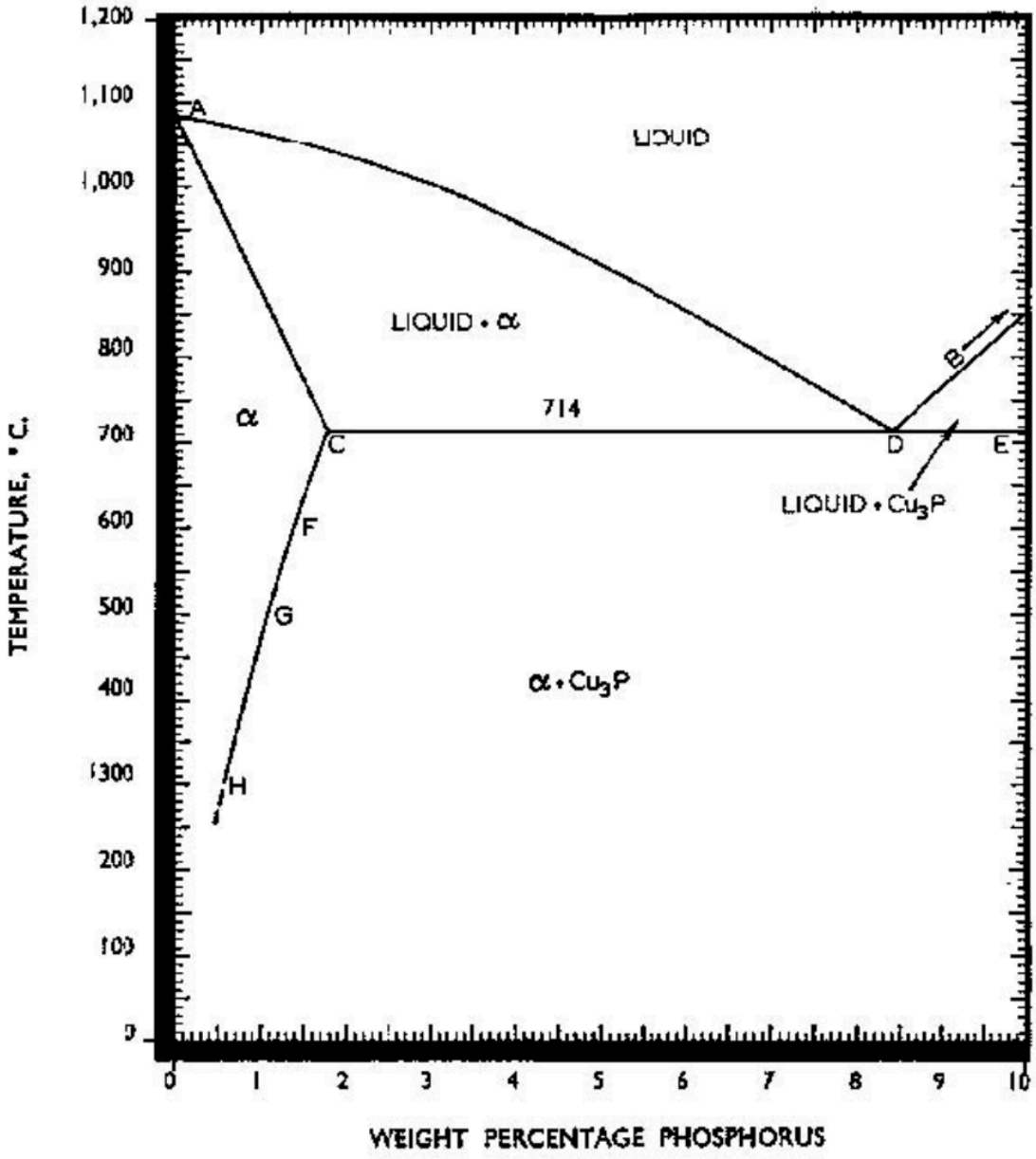

Figure 6: Part of the Phase Diagram of Cu-P with phosphorus concentration up to 10 wt%.

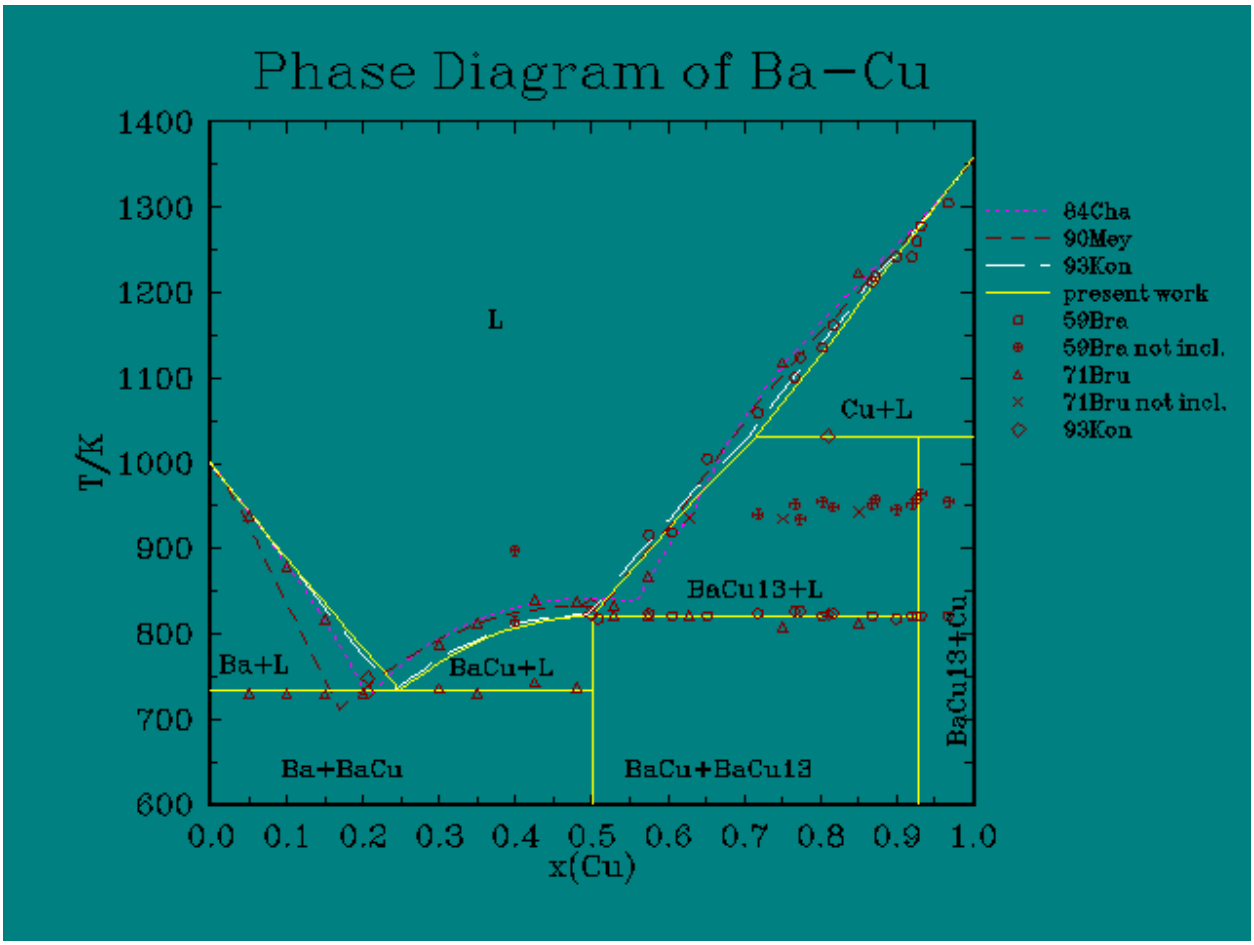

Figure 7: Phase Diagram of Ba-Cu.

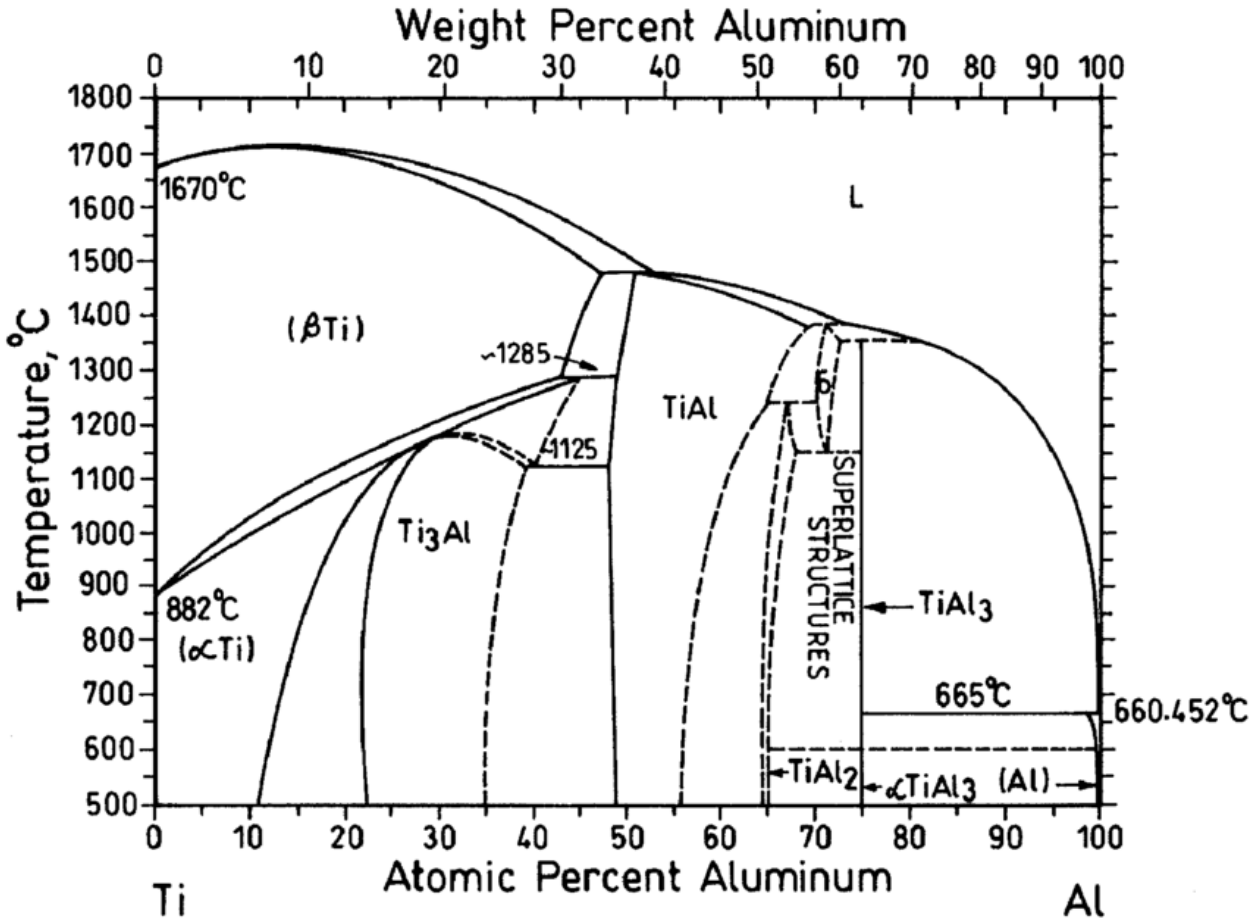

Figure 8: Phase Diagram of Ti-Al.

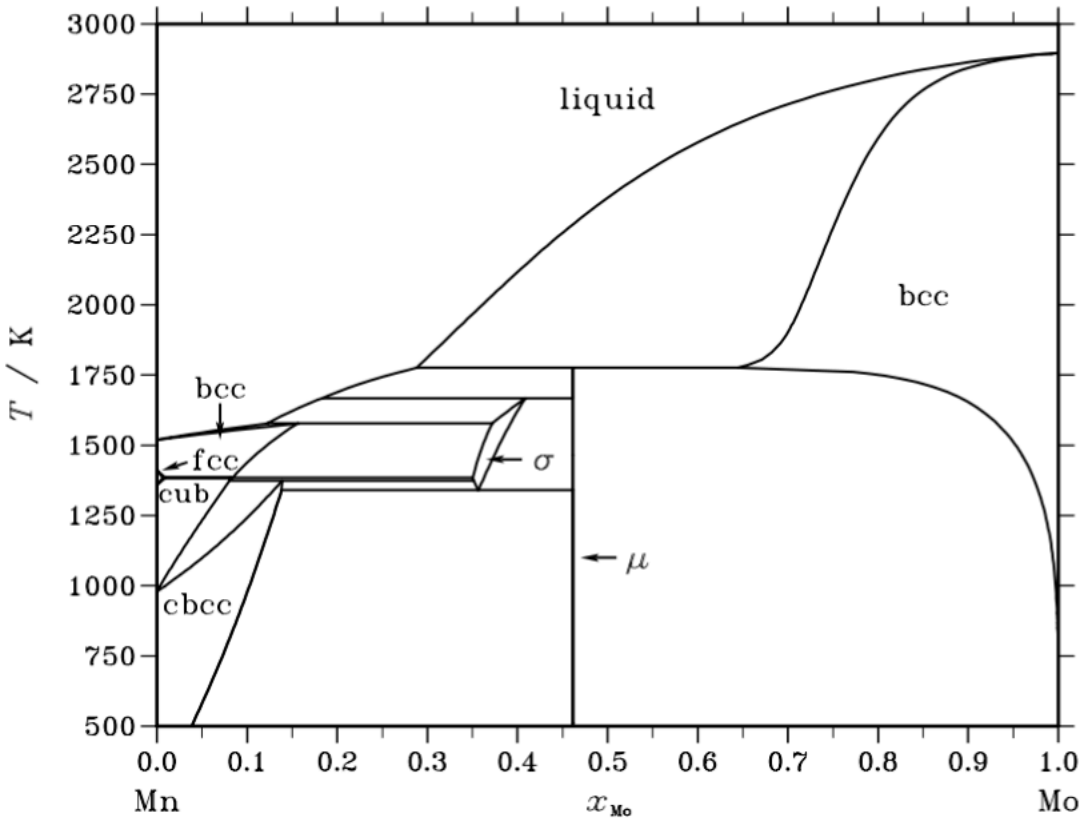

Figure 9: Phase Diagram of Mn-Mo.

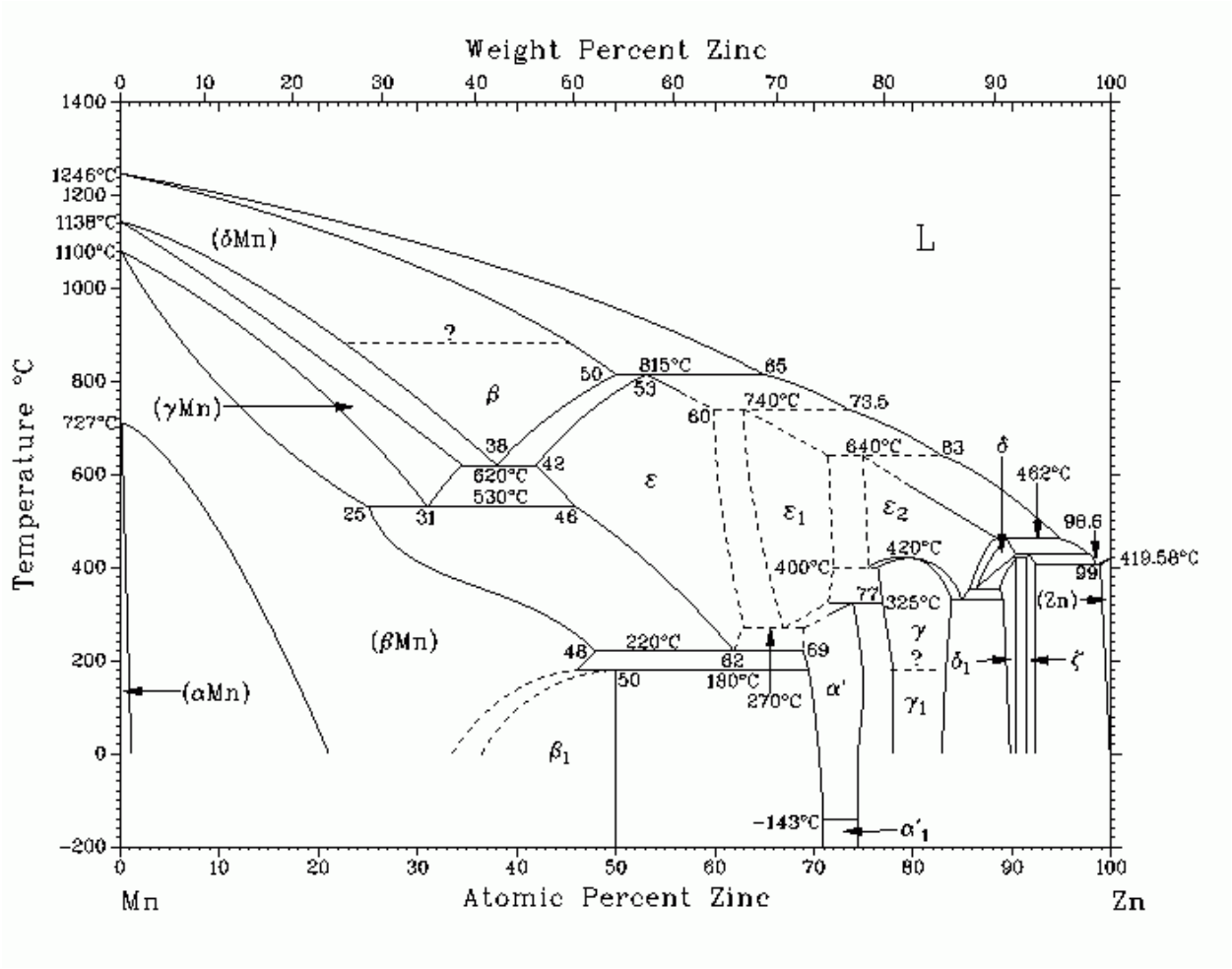

Figure 10: Phase Diagram of Mn-Zn.

CHAPTER 3

DIRECTIONAL SOLIDIFICATION OF CU-P-AG EUTECTIC ALLOY AND THE THERMAL PROPERTIES

3.1 Background

Directional solidified eutectic alloys are common structures of showing anisotropic properties in the solid phases. During phase change, the alloys become isotropic in the liquid phase [36]. After surveying all the binary alloys, the family of Copper-Phosphor (Cu-P) eutectic alloys brought our attention because they combines a high thermal conducting phase of copper and a low thermal conducting phase of phosphor alloy (usually semi-conducting) shown in Fig. 3 [7]. Not only this type of eutectic alloy show high thermal conductivity contrast along different directions, it also gives us another possible thermal conductivity contrast between the high temperature liquid phase and the low temperature solid phase.

Copper-Phosphor-Siliver (Cu-P-Ag) alloy is a widely used brazing alloy. It is cheap, abounded and having high fluidity. Although pure Cu-P eutectic alloy has very high working temperature, adding Ag to the binary alloy can lower the melting temperature up to 100 ^{o}C [37]. The solubility of Ag in the alloy limits how much the liquidus line can be lowered. Thus, adding too much Ag is not possible and would cause phase separation. The phosphor content increases the fluidity of the material, but too much phosphor also makes the alloy very brittle [38]. Considering both the mechanical and economical issues of this alloy, we choose to work with Cu-9.8%P-4.0%Ag for our thermal switch application. It contains phases of a copper rich phase αCu-Ag and a phosphor rich phase Cu_3P. The Copper rich phase has a face centered cubic (FCC) structure and the phosphor rich phase has a hexagonal crystal structure [39]. Therefore, we

expect to see the thermal conductivity contrast from different phases, structures, composition, and thermal boundaries using this alloy.

The main focus of Cu-P-Ag alloy previously was mainly studied on its electronic brazing application, especially in electronic packaging, and the unidirectional solidification has never done before [40]. Our material has a solidus temperature of 645^{o}C and a liquidus temperature of 720 ^{o}C. It is stable in air up to 150 ^{o}C, and can be heated up to 850 ^{o}C without decomposition according to manufacture [41]. We use these guidelines to directionally solidify our samples under different conditions.

3.2 Preparations and Characterization

3.2.1 Synthesis of the Directional Solidification Sample

The raw material Cu-9.8%P-4.0%Ag is purchased from Airgas, Inc named "Eutecrod 1804" in the circular rod form. We mechanically polish the rod using diamond film before experiment. We use a calendar lever to roll the rods multiply times into thin sheets around 350 μm. We then use a mechanical cutter to cut the sample into 1-inch long slabs for each individual test. To get rid of the oxidized copper outer layer before solidification, we polish the sample on diamond film again until the surface is shinny by naked eye, which usually takes 2 minutes on each side. Then, followed by sonication of the polished sample in water for 5 minutes, any dirt and debris are rinsed off of the polished surface. Two sapphire slides were cut and cleaned for holding the sample in between. The whole setup then put into a porcelain crucible for the heating experiment.

The next step is getting the furnace ready for directional solidification. We put the porcelain crucible into a quartz furnace, which is placed into a single zone furnace shown in

Figure 12. We then attach two copper sleeves at the two ends of the quartz tube to reduce heat flux hitting the gas tubes at the ends and providing sharp thermal gradient along the furnace from the center. After hooking the porcelain crucible up with the syringe pump, we seal the quartz tube and let argon gas flow.

The temperature cycle we use is shown in Table 1. We pick a starting position of the sample with thermal gradient being 6.1~6.3 ^{o}C/mm in the furnace. We flow argon gas at 60 ^{o}C in the first step to dry the sample from outside moisture and exchange the oxygen in the furnace to argon. Then, in the second step, we ramp the temperature up to 800 ^{o}C to completely melt the sample into liquid phase. Next, the sample is dragged using a syringe pump at a certain pulling speed along the furnace, which with a thermal gradient based on the starting temperature and the position of the copper sleeve. In the last step, we wait the furnace to naturally cool down to remove the sample. The pulling speeds we tried are between 1.59 mm/min and 15.9 mm/min.

3.2.2 Characterization and Preparation for the TDTR Experiment

After the directional solidification experiment, we usually do a scanning electron microscopy (SEM) experiment to determine the quality of the sample. If the structure is ordered in all directions by checking a few cross-sections, we can prepare the sample for TDTR measurement. We mark the lamellar growth direction from SEM, and polish one surface of our interest to optically smooth. The polishing steps are standard for TDTR experiment preparation. A piece of sample is glued on the sample holder using crystal bond. We use diamond films with various size subsequently: 9 μm, 6 μm, 3 μm, 1 μm, and 0.5 μm at last on MetaServ 250 polishing machine with water turned on. We polish the sample on each film for 5 min using speed of 80-100 rpm and very light hand pressure. After polishing, we wash the sample using

running water and watch the surface under an optical microscope to check on the smoothness and the directionality of structure.

Following the polishing step, the sample is put into a magnetron sputter machine to deposit aluminum metal on top of the polished surface with targeted thickness being 80 nm. The actually thickness can be calculated from the TDTR experimental data later, and aluminum serves as the metal transducer for our measurement.

3.3 Characterization of the Directional Solidified Cu-P-Ag Alloy

To start working with the sample, a lot of the material properties are crucial and necessary to be understood fully. We determine the crystal structures of the phases using XRD. The result is shown in Figure 14 with copper phase labeled as green lines and copper (I) phosphide (Cu_3P) labeled as blue lines. The structure of the directional solidified alloy is characterized using different techniques. One of the traditional ways of studying the structure is based on chemical etching on a smoothly polished surface. We find one recipe with fast and reliable etching rate [42]. The Klemm's II regent changes the color of the polished surface in a few minutes. After soaking, we raise the sample using generous amount of water to get rid of the debris and remaining etchant. Then we record the image of the surface before and after etching in an optical microscope to get the structure of phases. Figure 13 shows different parts of the surface before and after etching, from which we did not see any lamellar like structure, but circular pockets of one phase being etched away. Therefore, other techniques are required for more accurate understanding.

Since we cannot see the lamellar structure from the sample, we suspect that our Cu-P sample contains other impurities. However, the company that sells the raw material keeps other

components as trading secrets, so we only get to find out that it is actually Cu-P-Ag alloy from X-ray Fluorescence (XRF) measurement shown in Figure 15. In Fig. 15's plot, we have calculated the concentrations of each component with copper being 88.5 wt%, P being 7.3 wt%, and Ag being 4.2 wt%. The Ag component is the reason that regular lamellar is hard to form. One thing to note is that XRF is a topological measurement with certain confined beam size (1 cm in our measurement), so the actual distribution of the material may not be uniform. Our estimation based on measurements on different locations shown that the composition change between 1-2 wt%, which is a reasonable value for metal alloys.

Last but not least, we use Energy Dispersive X-ray spectroscopy (EDS) to further confirm the elemental distributions of all elements in the phases. We see from Figure 16 that the Ag component is only shown in the Cu rich phase region, and Cu_3P phase is more likely to form into bulky circular shape rather than the lamellar structure. Therefore, due to the nature of these phases, it is not suitable for making a phase changing thermal switch using this material.

3.4 Thermal Mapping Reflectivity Measurement of the Cu-P-Ag Alloy

To further understand the optical properties of the phases, we did a TDTR reflectivity measurement of the surface of the material. As shown in Figure 17(a), we picked a unique area of 100 μm with one phase forming an inverse Y shape from the optical microscope mode using TDTR. The beam size we chose was 5.5 μm. Then, a set of data was collected in the confined square along the horizontal (x-axis) with 40 steps and vertical (y-axis) with 40 steps. The V_{in}, V_{out}, V_{in}/V_{out}, and detector voltage are plotted via grey scaled color map. Since we did not deposit any metal transducer, the surface is not ideal to plot V_{in}/V_{out} along the phase boundary, scratches from polishing, or the lamellar region where two phases alternate consequently. We

have shown these odd values in red color in Fig. 17(d). In the detector voltage plot, we expect that the higher detector voltage would correspond to the copper phase and the lower detector voltage corresponding to the Cu_3P phase since copper has a reflectivity near 1. However, we did not see this trend from the plot. It is possible that since Cu_3P is florescence in the visible light, other types of secondary light is generated or scattered from the laser beam and being detected. We can confirm that the two phases have very distinct reflectivity. Hence, it is possible to extrapolate the difference in thermal conductivity of the two phases.

3.5 Thermal Conductivity Measurement of the Cu-P-Ag Alloy

For our bulk sample, we are interested in not only the thermal conductivities of different phases, we also want to know the average thermal conductivity of the bulk material, which provides the homogeneous state of the thermal switch at room temperature. Therefore, our first approach is a thermal measurement of the bulk material.

The average thermal conductivity we measured is 13.34 W/mK for the bulk using a laser beam size of 5.5 μm shown in Figure 18. Since the thermal conductivity of this material is not measured before, we calculated the thermal conductivity based on Weidemann-Franz Law to get a theoretical value around 40 W/mK with electrical conductivity measured using four point probe measurement to be $5.51X10^6$ S/m. Although the TDTR measurement is not consistent with the theoretical calculation, we suspect that our material contains other impurities and oxidations on the metal surface to further lower the thermal conductivity from the theoretical value.

3.6 Figures and Table

Table 1: Heating cycle for directional solidification experiment flowing in argon gas

Step	Time (hr)	Temp. (^{o}C)	Ramp (^{o}C/min)
1	0.5	60	1.2
2	3	60 to 800	4.1
3	0.5	800	HOLD
4	OFF	25	N/A

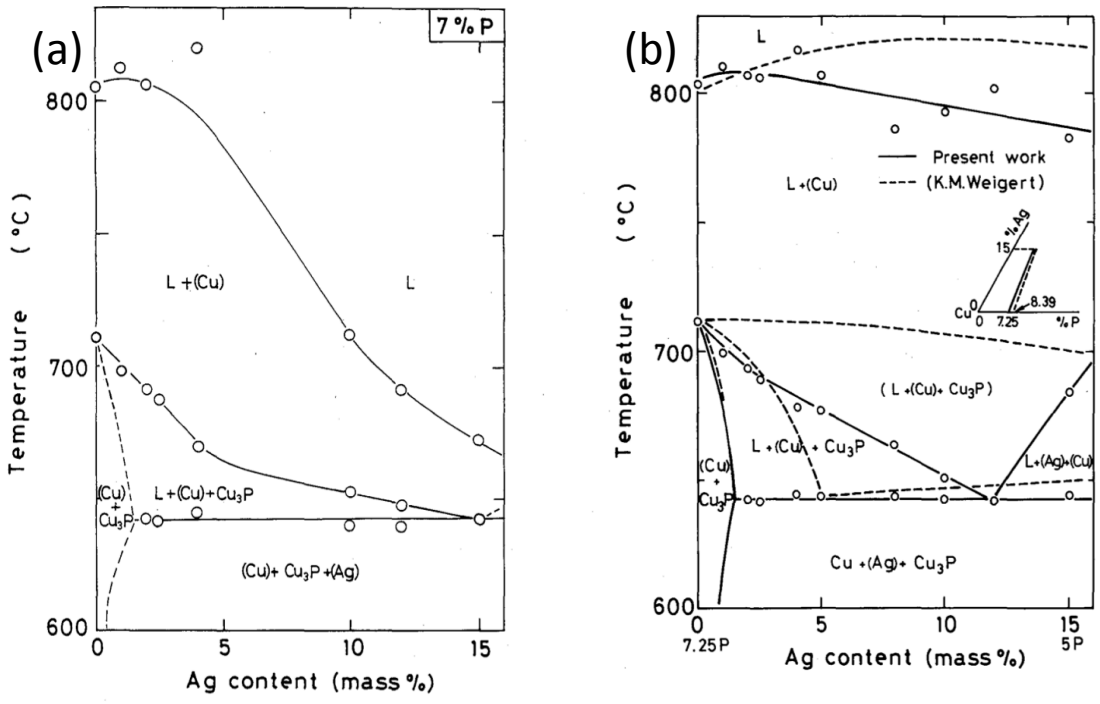

Figure 11: Phase diagram of Cu-P-Ag alloy (a) vertical section of Cu-P-Ag ternary phase diagram at 7% P (b) vertical section of Cu-P-Ag ternary phase diagram of Cu-7.25%P to Cu-5%P-15%Ag.

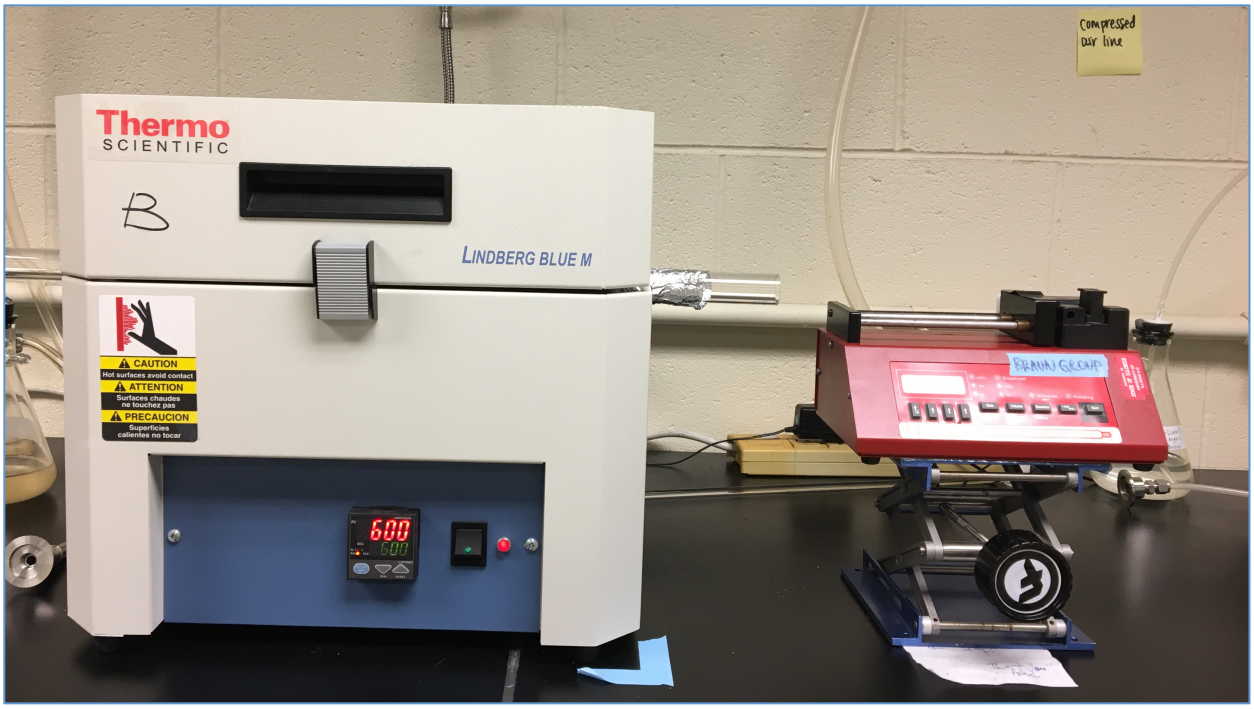

Figure 12: The setup of directional solidification.

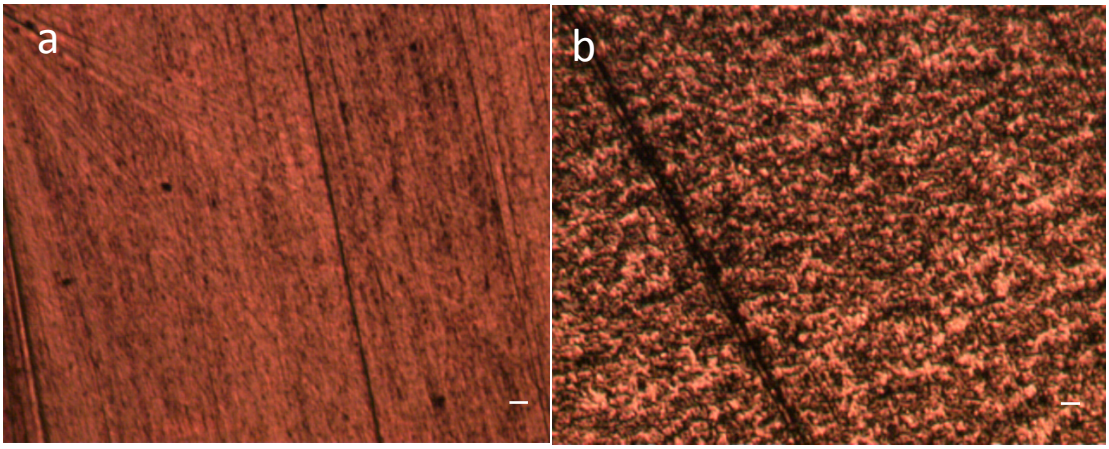

Figure 13: Tinted etched Cu-Ag-P alloy (a) optical microscope image of polished surface before etching (b) optical microscope image of the same surface after etching (scale bar size 10 nm).

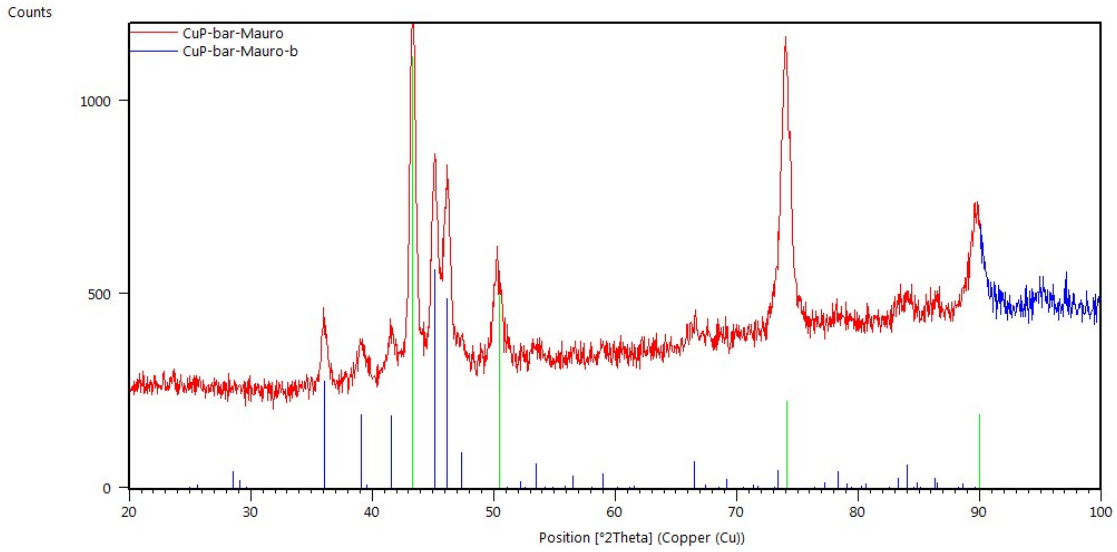

Figure 14: XRD measurement of the Cu-P-Ag alloy (green lines representing copper peaks and blue lines representing Cu_3P phases).

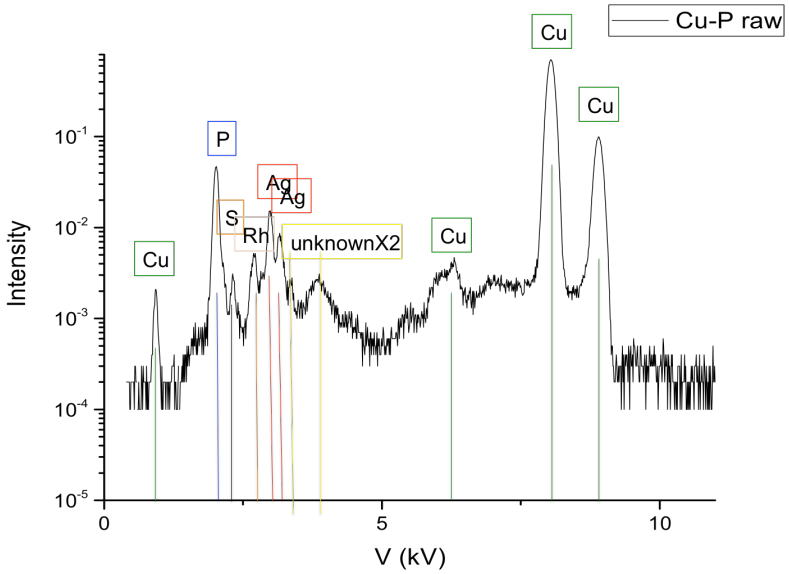

Figure 15: XRF plot of log scaled Cu-P-Ag raw sample with concentrations of Cu=88.5 wt%, P=7.22 wt%, and Ag= 4.2 wt%.

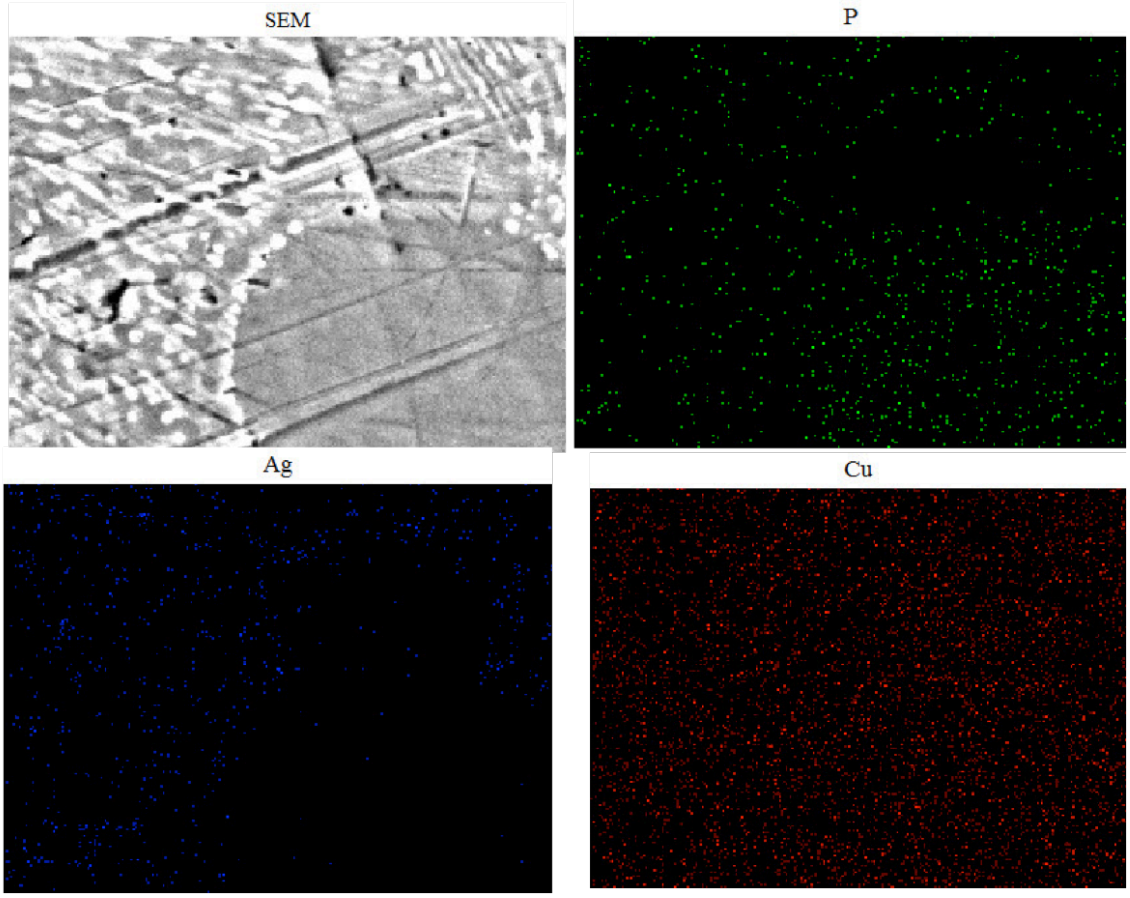

Figure 16: Energy Dispersive X-ray (EDS) spectroscopy analysis based on the SEM image (top left) of Cu-P-Ag sample. The phosphor, silver, and copper's position and concentration are represented by green, blue and red dots respectively.

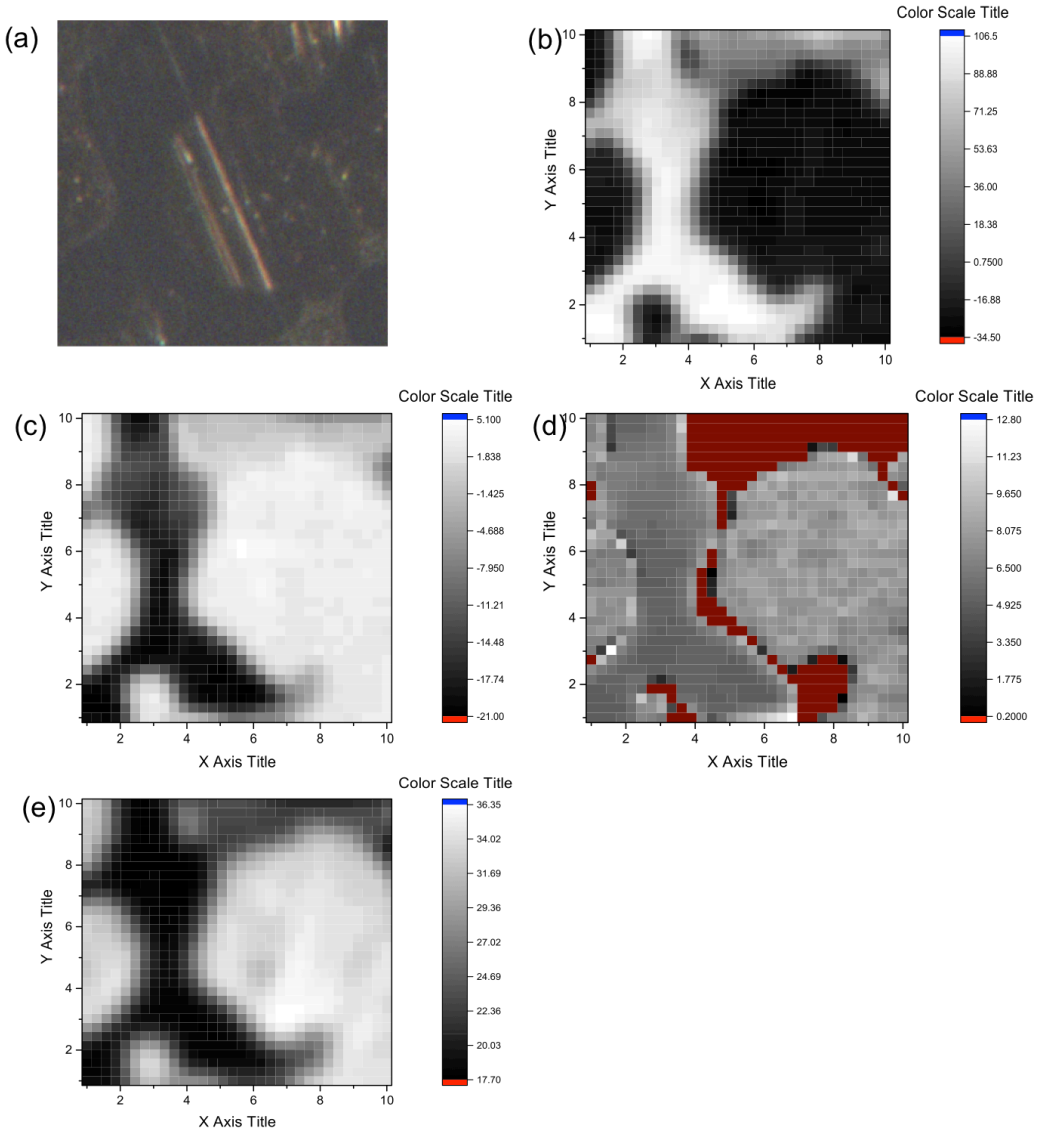

Figure 17: TDTR mapped area of the Cu-P-Ag sample with step size 2.5 μm and 40 steps along the x-axis and 40 steps along the y-axis (a) optical image of the mapped area, (b) V_{in} signal of the sample, (c) V_{out} signal of the sample, (d) V_{in}/V_{out} of the signal of the sample, and (e) detector voltage of the sample.

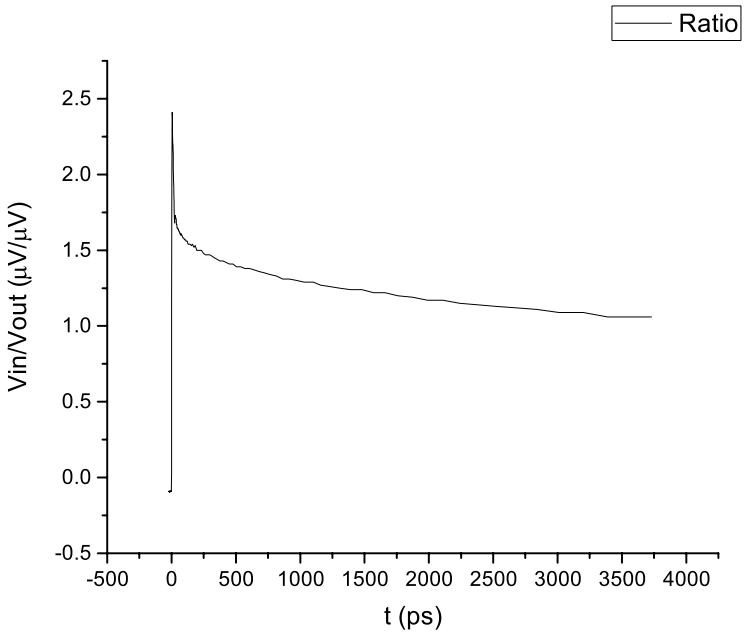

Figure 18: The data plot of thermal conductivity measurement from TDTR showing the ratio of V_{in} versus V_{out}. The thermal conductivity we measured is 13.34 W/mK.

CHAPTER 4

DIRECTIONAL SOLIDIFICATION OF CU-P EUTECTIC ALLOY AND THE THERMAL PROPERTIES

4.1 Background

Copper phosphorus (Cu-P) alloy is one of the most economical alloys for lots of engineering applications. From our research, depending on the area of application, Cu-P alloy is used as deoxidant, alloying and wetting agent, brazing alloy, and as nucleant with different amount of P concentration [43]. Most Cu-P alloy is added with other metals to increase its mechanical properties, such as adding silver to lower the melting temperature and increase the ductility, or containing iron due to the procedure of synthesis [44]. However, these types of alloys are hard to form into lamellar structure as we have discussed in chapter 3, so the pure Cu-P alloy is more suitable for our research.

The composition we are interested in for the directional lamellar structure is with 15.7 at.% (8.38 wt%) P [45]. As shown in Figure 19, it is one of the eutectic point compositions at the corresponding eutectic temperature of 714 ^{o}C. Two of the solid phases below the eutectic temperature are α-Cu phase and Cu_3P phase. The volumetric ratio between α-Cu phase and Cu_3P phase is 61% and 39% respectively based on our calculation, which is one way to ensure the possibility of getting directional lamellar structure, and gives us large ratio of anisotropic thermal conductivity. Therefore, we predict this material is a good candidate for our application.

4.2 Preparations and Characterization

4.2.1 Synthesis of the Directional Solidification Sample

We purchased the raw material from Osaka Alloy Works, Co.,LTD. The exact composition is 8.5 wt% P (slightly higher than the 8.38 wt% P eutectic composition). The sample was received as metal shots with irregular shapes, which brings difficulty to polish into thin sheets. It would be ideal to mechanically cut the shots into hundreds micrometer thin sheets using diamond saw for easy assembly in the directional solidification step, but we did not done it perfectly due to the limited time. What we have tried for cutting the shots into thin sheets is using Electrical Discharge Machining (EDM). It did not work well for our material because it got zinc contamination from the cutting wire into our sample with a zinc concentration around 10 wt%, and mechanical polishing off the top layer could not get rid of the contamination neither. We suspect that because of the fast diffusion rate of zinc, accumulation of zinc would not happen only on the surface. Therefore, we expect that we can get more systematic measurements after cutting the sample into confined shapes. The rest of the preparation steps are the same as what has been described in section 3.2.1 and the same apparatus as Fig. 12. The thermal gradient in the furnace we used is 6.1 ^{o}C/mm and the pulling speeds we tried are between 1.59 mm/min and 15.9 mm/min.

4.2.2 Characterization and Preparation for the TDTR Experiment

The TDTR experiment requires an optical degree polished surface with a thin film metal deposition as a thermal transducer. Before polishing the sample, we usually use SEM or optical microscope to identify the surface of interest (along or perpendicular to the growth of the lamellar direction), so we can polish the correct plane for our measurement. This step is usually

involves with lots of manual skills and time consuming using our technique, which is hand holding polishing using MetaServe 250 machine. Details about the polishing steps are the same as shown in Sec. 3.2.2. We expect that using Focused Ion Beam (FIB) machine would make this step more accurate and more efficient in future. After polishing, we rinse the sample three times using deionized water in sonicator for a few minutes to get rid of any remaining debris. Then, we use magnetron-sputtering machine to deposition Al as metal transducer (targeted thickness at 80 nm) to the polished surface.

Although the sample needs to be carefully prepared in TDTR experiment, once we got the prepared sample ready and calibrated the TDTR apparatus, the actual measurements can be repeated fast to get a reliable averaged value [46].

4.3 Characterization of the Directional Solidified Cu-P Alloy

The directional solidified results of the Cu-P sample are much more ordered than the Cu-P-Ag sample shown in Figure 20. We get straight lamellar structures in the solidification direction at large area of hundreds of micron meters. The spacing of lamellae (two phases together) we got is between 1.7 μm to 2.5 μm depending on different pulling speeds. In general, a slow pulling speed tend to make the lamellar spacing wider compared with a fast pulling speed in the range of 1.59 mm/min to 15.9 mm/min.

The polished surface used for lamellar spacing measurements and depositing the metal transducer is shown in Figure 21. We verified from EDS that the bright phase is the Cu rich phase and the dark phase is the Cu_3P phase.

The SEM images of the sample after directional solidification are shown in Fig. 20. From Fig. 20(a) and Fig. 20(b), we can see that the top surface is not completely flat due to different

surface tensions of the two phases, and the phases underneath the top runs straight downwards with no overlapping, which is an indication of directional thermal gradient. We can see the grating effect of light diffraction in the bulk in Fig. 20(c), which indicates large areas of the ordered lamellar structure. The lamellar spacing is a critical factor for eutectic/eutectoid materials to be used in optical area. For our application, it determines if we could use TDTR to measure one of the phases or the average of the two phases based on the beam spot size, and it also controls the thermal conductivities in different directions. To observe the structure growth of the cross section, we polished our sample down to the middle as shown in Figure 22. The growth direction is a little tilted from the perpendicular direction of the surface due to the direction of pulling is not always staying at the same angle for the porcelain container. The growth near the surface is much more straight shown in Fig. 22(a) than the inner part further away from the surface in Fig. 22(b) because the heat diffusion direction is less ordered in the center part. In future, it is the best to cut the sample into thin slices down to hundreds of micron meters. It would be the best to solidify the whole bulk sample with ordered lamellae in future with more refined parameters, but for now, the ordered area is good enough for our measurement.

4.4 Thermal Conductivity Measurement of the Cu-P Alloy

We measured the thermal conductivity of the directional solidified Cu-P alloy. With the TDTR beam size chosen to be 5.5 μm, the thermal conductivity perpendicular to the lamellar direction is 8.23 W/mK using one sample with average lamellar spacing around 2 μm, which is an average thermal conductivity of the two phases since the beam size is significantly larger than the lamellar spacing. We did not get a reliable thermal conductivity value along the lamellar direction. The reason is that it is hard to predict and polish perfectly along the lamellar plane in a

tilted solidified angle, and the penetration depth of TDTR is not deep enough to cover an average of the two phases, if we are not sure which phase is on the top surface and the thickness of the top surface. For future studies, it is the best to use FIB to do the polishing under SEM, so we can have more precise control. In addition, trying other thermal conductivity methods like Scanning Thermal Microscopy (SThM) and 3-omega thermal measurement may work better than TDTR because of larger penetration depth.

4.5 Figures

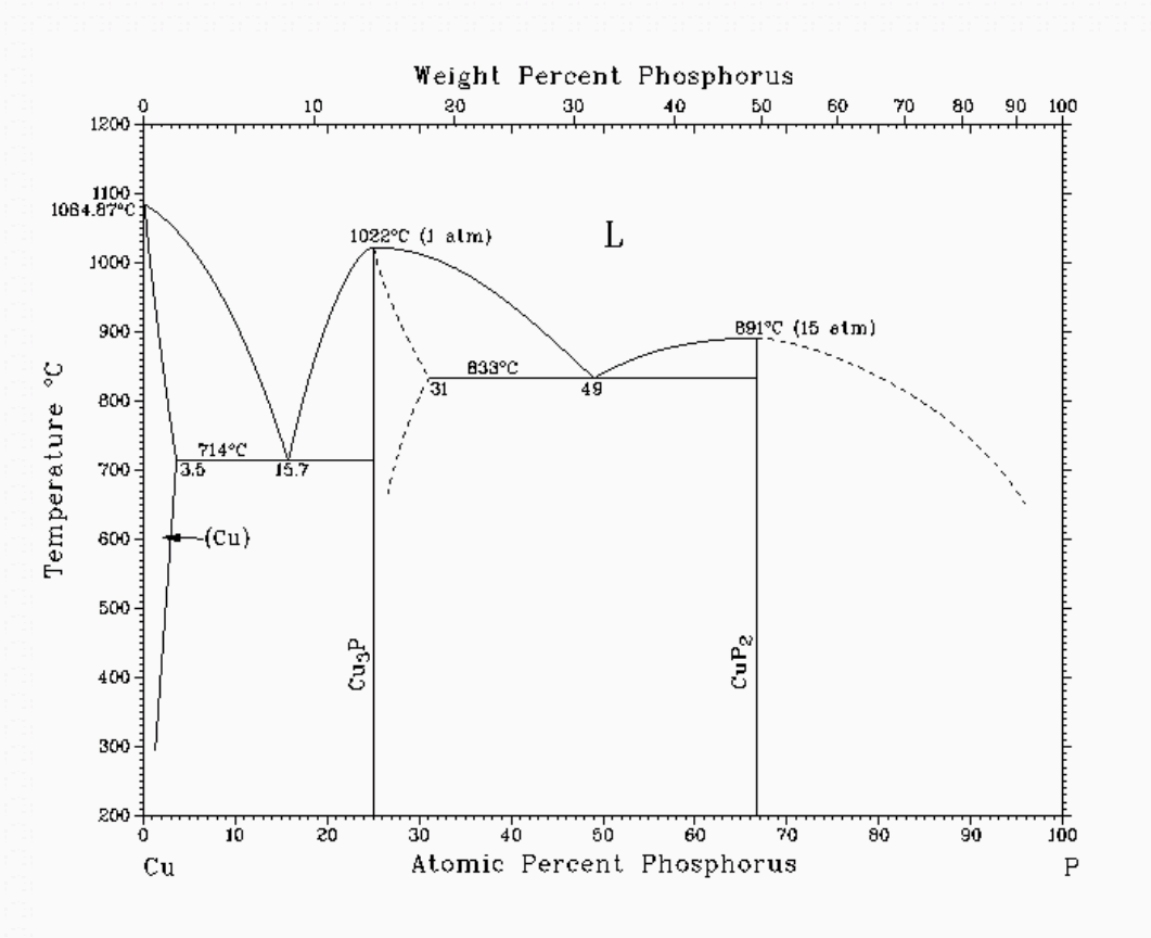

Figure 19: Phase diagram of Cu-P alloy.

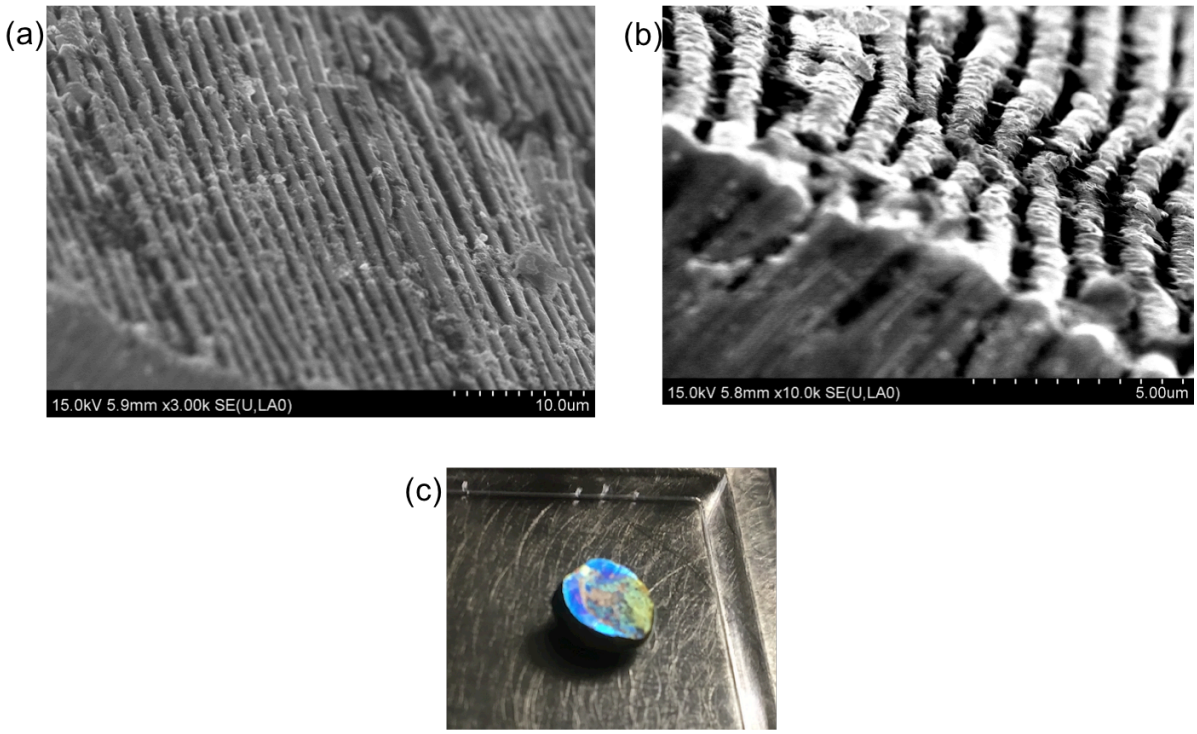

Figure 20: The directional solidified sample using a pulling speed of 15.9 mm/min (a) top surface without polishing, (b) the cross-section of the sample, (c) the sample after experiment showing light reflections.

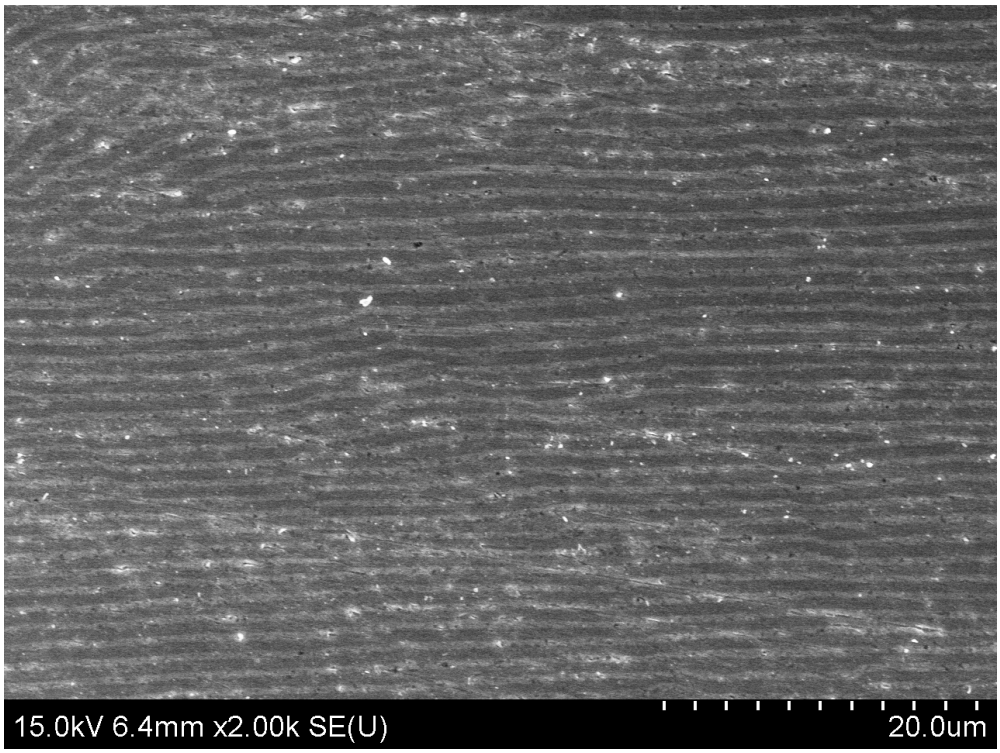

Figure 21: Directional solidified top surface with pulling speed of 1.59 mm/min.

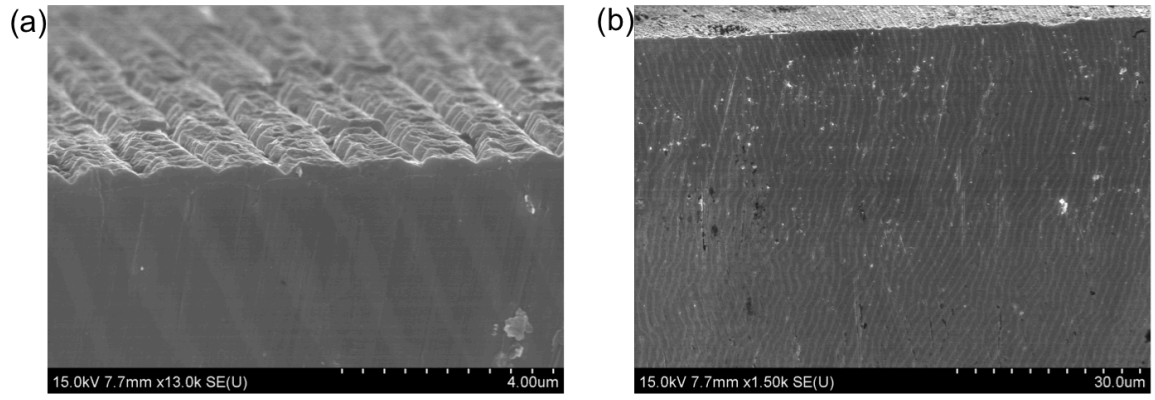

Figure 22: Cross-section of the directional solidified Cu-P sample.

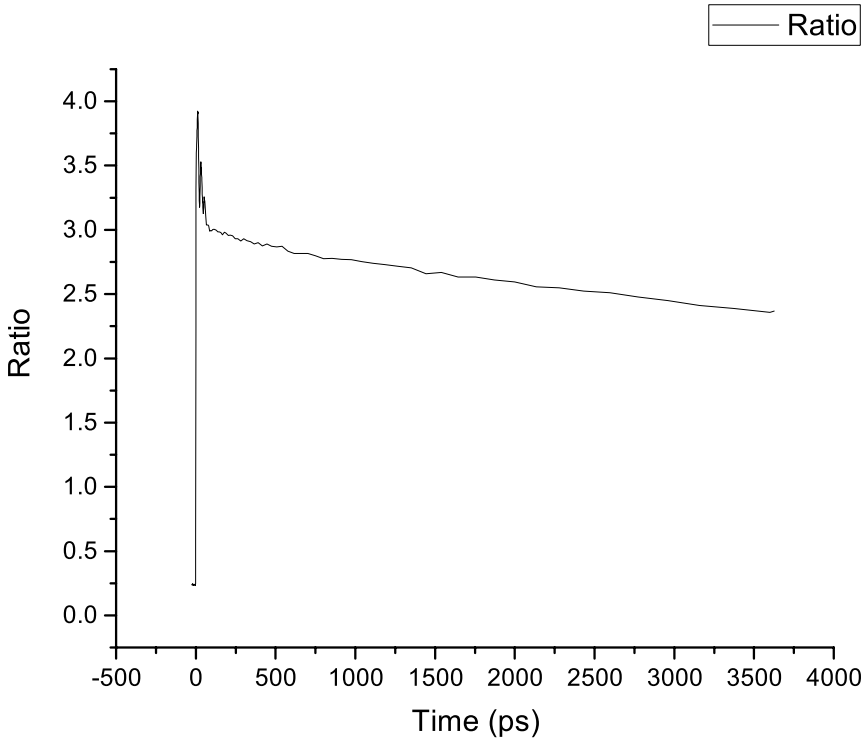

Figure 23: The TDTR thermal conductivity measurement of the directional solidified Cu-P sample. The ratio is shown using data values of V_{in}/V_{out}. The thermal conductivity through the top surface (along the lamellar direction) is measured to be 8.23 W/mK.

CHAPTER 5

CONCLUSION

In this thesis, we have surveyed all the binary alloys, and find several candidates in the eutectic and eutectoid categories for thermal switching applications. We have predicted the thermal conductivity of each candidate from known values and theories. The structures upon phase changing of many of these alloys are not studied previously. Therefore, directional solidification of these candidates would be interesting topics alone or combined with other anisotropic property applications like thermal switching.

We have demonstrated a simple method to direction solidify eutectic alloys. Two of the samples we have tried are Cu-P-Ag alloy and Cu-P eutectic alloy. The Cu-P-Ag sample is difficult to directional solidify due to the nature that Cu rich phase prefers to form isolated circular pockets rather than lamellar. The structure of Cu-P eutectic alloy shows good lamellar directionality with spacing between 1.7 μm to 2.5 μm depending on different pulling speeds and different thermal gradients. The ordered lamellar structure we have achieved is about hundreds of micrometers. Hence, with further refining the parameters and sample sizes, the ordered structure can be increased to fit different applications.

For both of Cu-P-Ag and Cu-P eutectic samples, we have done the thermal conductivity measurements via TDTR. Cu-P-Ag has a bulk thermal conductivity of 13.34 W/mK. Cu-P has an in-plane thermal conductivity of 8.23 W/mK, and the out-of-plane thermal conductivity can be measured accurately with fine polishing in future. In addition, other thermal conductivity methods like Scanning Thermal Microscopy (SThM) and 3-omega thermal measurement may be helpful as comparisons values.

REFERENCE

[1] "The Iron-Carbon Phase Diagrams." *Teach Yourself Phase Diagrams*, www-g.eng.cam.ac.uk/mmg/teaching/typd/addenda/definition.html.

[2]"Eutectic". BusinessDictionary. Web Finance Inc. 2017.

[3] Nelson, Stephen A. "Experimental Determination of 2-component Phase Diagrams." *Component Phase Diagrams*. Tulane University.

[4] "Introduction to Material Science." *Chapter 9*, University of Tennessee, 2003.

[5] Büyük, U., S. Engin, and N. Maraşlı. "Directional Solidification of Zn-Al-Cu Eutectic Alloy by the Vertical Bridgman Method." Journal of Mining and Metallurgy, Section B: Metallurgy51.1 .2015. 67-72.

[6] Pawlak, D. A., G. Lerondel, I. Dmytruk, Y. Kagamitani, S. Durbin, P. Royer, and T. Fukuda. "Second Order Self-organized Pattern of Terbium–Scandium–Aluminum Garnet and Terbium–Scandium Perovskite Eutectic." Journal of Applied Physics91.12. 2002. 9731.

[7] Smith, Hashemi. Foundations of Materials Science and Engineering. McGraw-Hill. 2006.

[8] Ke, Yangchuan, et al. *Crystallization, Properties, and Crystal and Nanoscale Morphology of PET–clay Nanocomposites*. Journal of Applied Polymer Science, 8 Jan. 1999.

[9] *Self-Assembled Nanometer Lamellae of Thermoelectric PbTe and Sb2Te3 with Epitaxy-like Interfaces*. ACS Publications, Jan. 2007.

[10] Cieszynski, Fox. Electronics for Service Engineers,Routledge. 1999. ISBN 0750634766, p.175

[11] "Fire Sprinkler and Suppression System Design, BIM Coordination and 3D Modeling, Fire Pump and Standpipe design." *Fire Sprinkler Design*, 3D Fire Desgin LLC.

[12] Ng, Boon T., Zhi Y. Lim, Yew Mun Hung, and Ming K. Tan. "Phase Change Modulated Thermal Switch and Enhanced Performance Enabled by Graphene Coating." RSC Adv.6.90. 2016.

[13] Schmidt, A. J. Pump-Probe Thermoreflectance. *Annu. Rev. Heat Transf.* 16, 159–181. 2013.

[14] Cahill, D. G. et al. Nanoscale Thermal Transport. J. Appl. Phys. 2003, 93, 793.

[15] Cahill, D. G., Fischer, H. E., Klitsner, T., Swartz, E. T. & Pohl, R. O. "Thermal Conductivity of Thin Films: Measurements and Understanding". *J. Vac. Sci. Technol. A* **7,** 1259–1266. 1989.

[16] Cahill, D. G. "Thermal Conductivity Measurement from 30 to 750 K: the 3ω Method". *Rev. Sci. Instrum.* 61, 802–808. 1990.

[17] Bourlon, A. B., Van der Tempel, L. "Thermal Conductivity Measurement by the 3omega Method". Philips Research Repository.

[18] Mishra, V., Hardin, C. L., Garay, J. E., Dames, C. "A 3 omega Method to Measure an Arbitrary Anisotropic Thermal Conductivity Tensor". *Rev. Sci. Instrum.* 86, 54902. 2015.

[19] Cahill, David G, et al. "Comparison of the 3ω Method and Time-Domain Thermoreflectance." MRL, University of Illinois at Urbana Champaign.

[20] Lankford, K. "Heat Switches." *Semantic Scholar*, Semantic Scholar.

[21]Sobel, Dava. Longitude. London: Fourth Estate. p. 103. ISBN 0-00-721446-4.

[22] H. Lo, E. Chua, J. C. Huang, C. C. Tan, C.-Y. Wen, R. Zhao, L. Shi, C. T. Chong, J. Paramesh, T. E. Schlesinger, and J. A. Bain, "Three-Terminal Probe Reconfigurable Phase-

Change Material Switches", Electron Devices, IEEE Trans., vol. 57, no. 1, pp. 312–320, 2010.
[23] Jonstrup, Anette, et al. "DNA Hairpins as Temperature Switches, Thermometers and Ionic Detectors." Sensors, vol. 13, no. 5, Oct. 2013, p. 5937–5944. doi:10.3390/s130505937.
[24] Massalski, Thaddeus B., et al. *Binary alloy phase diagrams*. ASM International, 1992.
[25] Matveeva, N. M., and È V. Kozlov. *Ordered Phases in Metallic Systems*. Nova Science Publishers, 1996.
[26] Tadashi, Okamoto, and Matsumura. "Phase Diagrams of Cu-Ag-P and Cu-Sn-P Ternary Filler Metals. Copper Phosphorus Brazing Filler Metals with Low Melting Temperatures. Report II." Quarterly Journal Of The Japan Welding Society5.1. p. 81-86. 1987.
[27] "Thermal Conductivity of Common Materials and Gases." *The Engineering ToolBox*.
[28] Sun, Zijun, et al. "Copper Phosphide Modified Cadmium Sulfide Nanorods as a Novel p–n Heterojunction for Highly Efficient Visible-Light-Driven Hydrogen Production in Water." *Journal of Materials Chemistry A*, The Royal Society of Chemistry, 15 Apr. 2015.
[29] Aselage, Terry, and Keith Keefer. "Liquidus Relations in Y–Ba–Cu Oxides | Journal of Materials Research." *Cambridge Core*, Cambridge University Press, 1 Jan. 2011.
[30] Cahn, John W. "Alloys in Metastable Equilibrium." Bulletin of Alloy Phase Diagrams, vol. 1, no. 2, p. 26.1980.
[31] Das, Karabi, et al. " The Al-O-Ti (Aluminum-Oxygen-Titanium) System." ChemInform. Apr. 2003.
[32] "Titanium Alloys - Physical Properties." *AZo Materials*, 11 Aug. 2015.
[33] Zh. Fiz. Khim. 1996, v. 70, N 6, p. 986-990. Russ. J. Phys. Chem. (English transl.), 1996, v. 70, N 6.
[34] "Critically Evaluated Phase Diagrams", *The Bulletin of alloy phase diagrams*. 4th ed., v. 11, American Society for Metals, 1985.
[35] Cho, et al. "Enhanced Thermal Conductivity by Mn-Zn Ferrite Ferrofluids". 12th International Conference on Magnetic Fluid. 2010.
[36] "Chapter 9. Phase Diagrams", Materials Science and Engineering. Virginia University.
[37] "Copper Phosphorus (Cu-P) Alloy". READE international Corp.
[38] Landolt, H., and R. Börnstein. Thermodynamic properties of inorganic materials. Berlin, Springer, 1999.
[39] "Study on Low Silver Sn-Ag-Cu-P Alloy for Wave Soldering." *IEEE Xplore*, IEEE.
[40] Misawa, et al. "The Mechanism of Atmospheric Rusting and the Effect of Cu and P on the Rust Formation of Low Alloy Steels." *Corrosion Science*, Pergamon, 21 Nov. 2006.
[41] Bao, et al. "Strengthening Effect of Ag Precipitates in Cu–Ag Alloys: A Quantitative Approach". *Materials Research Letters*, 2016.
[42] Voort. "Copper Color Metal". Advanced materials and processes.
[43] Agresti, J., et al. "Development and Application of a Portable LIPS System for Characterizing Copper Alloy Artefacts." *SpringerLink*, Springer-Verlag, 27 Aug. 2009.
[44] Salvo, et al. "One-Step Brazing Process to Join CFC Composites to Copper and Copper Alloy." *Journal of Nuclear Materials*, North-Holland, 19 Aug. 2007.
[45] *Copper and Copper Alloy: Plate, Sheet, Strip and Circles for General Purpose*. BSI, 1998.
[46] *10th International Symposium on Measurement Technology and Intelligent Instrument, ISMTII 2011: June 29 - July 2, 2011, KAIST, Daejeon, Korea ;*Lab. for Precision Engineering and Metrology, KAIST, 2011.